Hindawi
Shock and Vibration
Volume 2018, Article ID 9213503, 26 pages
https://doi.org/10.1155/2018/9213503

Research Article

Comparative Study on Non-Gaussian Characteristics of Wind Pressure for Rigid and Flexible Structures

Lei Jiang,[1] **Jin-hua Li**,[2] **and Chun-xiang Li**[1]

[1]*Department of Civil Engineering, Shanghai University, Shanghai 200444, China*
[2]*Department of Civil Engineering, East China Jiaotong University, Nanchang 330013, China*

Correspondence should be addressed to Chun-xiang Li; li-chunxiang@vip.sina.com

Received 13 May 2017; Revised 17 August 2017; Accepted 23 October 2017; Published 17 January 2018

Academic Editor: Marco Belloli

This paper summarizes a comprehensive study for non-Gaussian properties of wind pressure. The field measurements are implemented on the structure surface of a rigid structure, while a large-span membrane structure is selected as the flexible structure wind pressure contrast group. The non-Gaussian characteristics of measured pressure data were analyzed and discussed through probability density distribution, characteristic statistical parameters, power spectral density function, and the correlations, respectively. In general, the non-Gaussian characteristics of wind pressure present depending on tap location, wind direction, and structure geometry. In this study, the fluctuating wind pressures on the windward side and leeward side of the structures show obvious different degrees of non-Gaussian properties; that is, the surface of rigid structure shows strong non-Gaussian property in leeward, while the roof of flexible structure shows obvious non-Gaussian property in windward. Finally, this paper utilizes the present autospectrum empirical formula to fit the wind pressure power spectrum density of the measured data and obtains the conclusion that the existing empirical formula is not ideal for fitting of the flexible structure.

1. Introduction

Wind loads possess stochastic characteristics, especially the fluctuating component, which may force the engineering structure to flutter, torsional vibration, and other forms of wind-induced random coupling vibration. In the 1970s and 1980s, research on characteristics of wind load on structural has begun; Dalgliesh [1] computed the pressure coefficients of measured wind pressures to better identify potential problem areas on high-rise building. Holmes [2] compared correlations and spectra of pressure fluctuations on the windward and leeward faces of a 43 m high building and found the error of quasi-steady linear theory. Stathopoulos and Surry [3] made a contribution to the question of scaling for low building models in wind-tunnel experiments. Nevertheless, they did not consider the problem of the non-Gaussian characterization of wind pressures. In some separate flow regions, the wind pressure distributions show obvious non-Gaussian characteristics [4–6] due to the influence of air separation, reattachment, and vortex shedding. This kind of wind pressures with asymmetric distribution and sharply pulse peak, which has close correlations with the vortex movement of the wind field, leads easily to the fatigue damage of structure and is the major cause of local structural damage [7]. Compared with the Gaussian wind pressures, the non-Gaussian wind pressures take on the feature of asymmetric and/or leptokurtic distribution, which is the nonnormal distribution. Many researchers have contributed to research on non-Gaussian processes [8–13]. Kumar and Stathopoulos [4, 5] expounded the existence of the non-Gaussian wind pressures on the flat and herringbone roofs of low-rise building and conduct the partitions of the Gaussian and non-Gaussian areas. Through a wind-tunnel test, Ye and Hou [6] tested that wind pressure shows obvious non-Gaussian characteristics on the windward edge area and the corner of long span roof and partitioned the non-Gaussian region of wind pressure using the curve fitting method based on the *K-S* test. Through a wind-tunnel test on rhombus super high-rise buildings along with chamfers, Lou et al. [14] partitioned the Gaussian and non-Gaussian distributions of

fluctuating wind pressures on the structural surfaces under consideration of different wind direction angles, respectively, and found that there exist remarkable non-Gaussian wind pressures on the flow separation zone of lateral inlet edge and the incisal angle region of leeward and windward side. The non-Gaussian characteristics of pulsating wind pressures on square high-rise buildings were researched by Han and Gu [15] through a wind-tunnel test; the results show that non-Gaussian characteristics are prominently affected by the wind angle. On the windward surfaces, both positive skewness and negative skewness of the wind pressures are present, and the kurtosis and skewness values are relatively small. On the surfaces impacted by separated flow and wake, only negative skewness is present; both kurtosis and skewness values are relatively large. Recently, a new moment-based polynomial model for coping with hardening non-Gaussian processes with kurtosis less than three was presented in Ding and Chen's work [16]. Ma et al. [17] presented a hybrid data and simulation-based (HDSB) approach that incorporates simulated data based on an autoregression (AR) model with an inverse Johnson transformation to estimate the extreme values of non-Gaussian wind pressures.

Previous studies on the non-Gaussian characteristics of wind pressures are mainly conducted through wind-tunnel test data, while the field measurement data of non-Gaussian wind pressure is very limited. Li et al. [18] investigated the characteristics of tropical cyclone-generated winds and evaluated the wind effects on a typical low-rise building under tropical cyclone conditions through field measurements.

Large-span membrane structure, as a new appearance structure, has superior mechanical properties and light transmission. Some researchers [19–22] have done research on it. Bartko et al. [19] collected the wind speed, wind direction, and wind pressure field measuring data for extended time periods to analyze the wind interaction with low slope membrane roofs. Zheng et al. [21] simulated the mean wind load on the long-span membrane roof of the EXPO-axis by adopting Realizable k-ε turbulent model and investigated the effects of surrounding buildings on the mean wind pressure distribution on the membrane. Luo et al. [22] presented a zero memory nonlinearity (ZMNL) transformation based method to simulate the stochastic fluctuating wind pressure field acting on a large-span membrane roof, which consists of Gaussian and non-Gaussian regions. However, academics have yet to systematically discuss the non-Gaussian property of the flexible structure; it is thus urgent to investigate.

The power spectrum of pulsating wind pressure is based on a limited data collection to describe the power (on the frequency) distribution of fluctuating wind pressure. Many scholars [23–30] have done some research on fitting the wind pressure autospectra data with empirical formulas. The universal model of wind velocity autospectra has been described by Olesen et al. [31] and Tieleman [32] as follows:

$$\frac{f \cdot S_P(f)}{\sigma_P^2} = \frac{A \cdot (f \cdot X)^{\gamma}}{\left(C + B(f \cdot X)^{\alpha}\right)^{\beta}}, \quad X = \frac{L}{U}, \tag{1}$$

where f is frequency in Hz; $\sigma_P^2 = \int_0^{\infty} S_p(f)df$ is the variance of wind velocity (or wind pressure); X is the fitting parameter; L is a feature length in m, which can be selected as the height of the structure or a constant length over the entire height; U is mean wind velocity in m/s. Li et al. [29] found that coefficient parameters, A, B, and C, are related to the location of the autospectral curves and index parameters, α, β, and γ, are related to the shape of the curve. Sun [26] and Pan [27] applied (1) in empirical formula of wind pressure autospectral model with identified parameters $C = 1$, $\alpha = 2$, and $\gamma = 1$ in Sun [26] and $\alpha = 10/3$, $\beta = 1$, and $\gamma = 1$ in Pan [27], respectively. With the aim of building an aerodynamic database for engineering application, Sun et al. [33, 34] and Shao [35] have made large amounts of wind-tunnel tests on large-span roofs, and the spectra of these wind pressure data were fitted with the wind pressure autospectral formula as follows:

$$\frac{f \cdot S_P(f)}{\sigma_P^2} = \frac{A \cdot f \cdot X}{\left(1 + B(f \cdot X)^2\right)^{\beta}}, \quad X = \frac{L}{U}. \tag{2}$$

This paper summarizes a comprehensive study for non-Gaussian properties, in which wind pressure time series is measured at different locations on two types of structure: the structure surface of a rigid structure and the roof of a flexible structure. Probability density distribution, characteristic statistical parameters, and the correlations of the measured pressure data were analyzed and discussed. Finally, this paper utilizes the present autospectrum empirical formula to fit the wind pressure power spectrum density of the measured data.

2. Statistical Parameters of Non-Gaussian Stochastic Process

According to the theory of random process, the first four-order statistical parameters, the mean, variance, skewness, and kurtosis, are the mathematical characteristics of random variables. For the random Gaussian process, the probability density function can be determined by only using the first two-order statistics parameters (i.e., the mean and variance), while it is very difficult for the non-Gaussian stochastic process. It needs high-order statistics parameters such as the third-order, fourth-order, or higher-order ones [36].

The mean $\mu = \overline{w} = \int_{-\infty}^{+\infty} wp(w)dw$ is the center of random process, which takes 0 value in the fluctuating random process. And the variance $\sigma^2 = \int_{-\infty}^{+\infty} w^2 p(w)dw$ is the degree of the deviation from the center. The third-order and fourth-order statistics parameters, namely, the skewness SK and kurtosis K, are used to describe the asymmetry and flatness degree of the distribution centered on the mean value, respectively. They can be stated as follows:

$$\begin{aligned} \mathrm{SK} &= \sigma^{-3} \int_{-\infty}^{+\infty} w^3 p(w)\, dw \\ K &= \sigma_w^{-4} \int_{-\infty}^{+\infty} w^4 p(w)\, dw, \end{aligned} \tag{3}$$

Figure 1: Effect drawing of Yueqing Sports Center.

where $p(w)$ is the probability density function of stochastic process w.

Treated as a random process, the discrete random fluctuating wind pressure $\{P_i \mid i = 0, 1, 2, \ldots, N-1\}$ can be characterized by the following four-order statistics parameters:

$$\begin{aligned} \mu &= \frac{1}{N}\sum_{i=0}^{N-1} P_i \\ \sigma^2 &= \frac{1}{N}\sum_{i=0}^{N-1} P_i^2 \\ \mathrm{SK} &= \frac{(1/N)\sum_{i=0}^{N-1} P_i^3}{\left((1/N)\sum_{i=0}^{N-1} P_i^2\right)^{3/2}} \\ K &= \frac{(1/N)\sum_{i=0}^{N-1} P_i^4}{\left((1/N)\sum_{i=0}^{N-1} P_i^2\right)^{2}}. \end{aligned} \tag{4}$$

The skewness and kurtosis of Gaussian stochastic processes are fixed. A skewness value of zero and a kurtosis of 3 mean that the stochastic process follows normal distributions; otherwise it is a non-Gaussian stochastic process. For the skewness value, when it is greater than 0, the distribution curve is positive skewness, and the long tail of the curve is in the positive direction of the horizontal axis; when it is less than 0, the curve is negative skewness, and the long tail is in the negative direction. For the kurtosis value, when it is less than 3, the distribution curve is lower than the normal curve; when it is greater than 3, the curve is steeper than the normal curve.

3. Field Measurement Program and Data Analysis

3.1. Flexible Structure Field Measurement. Yueqing City Sports Center is located in Xu Yang Road, Yueqing City, which is composed of the stadium, swimming pool, and gymnasium. The stadium building is about 229 m from north to south, 211 m from east to west, and about 42 m from the top of the column. The roof is covered with meniscus nonenclosed space cable-truss system. The maximum cantilever span is about 57 m. The wave structure of the membrane structure is supported by the 273 × 10 steel pipe arch of the cable-truss system. Under the structure of the two waves, the rope structure is arranged under the cable. The effect of the stadium is shown in Figure 1.

Zhi-hong et al. [37] have started Yueqing Sports Center stadium membrane surface of the overall pressure measurement study on 25 December 2012. The installation and commissioning are started in mid-April 2013; the wind speed, wind direction, and wind pressure data measured under the strong wind/typhoon will be open to the world. The stadium has a total of 38 cable girders, with 3 corners of the stadium each without paving. According to the rigidity model test results of wind tunnel and the general law of flow field separation and evolution, the layout of wind pressure measurement points on the membrane surface is shown in Figure 2. The wind pressure sensor is installed at the top and bottom of each measuring point, and the wind pressure time course of the upper and lower surface of the membrane can be monitored synchronously. Wind pressure monitoring system equipment mainly includes lightning-type wind load sensor CYG1721 (top surface) and the mine-type differential pressure sensor CYG1722 (lower surface), 256-channel sampler, and shielding gas lead waterproof cable; the specifications of the device model are given in Table 1.

Wind pressure equipment on-site layout is shown in Figure 3. The geodetic coordinates of the 21 measuring points on the middle three pieces of the membrane structure for the sampling and the measured wind pressure data corresponding to the upper and lower membrane surfaces were achieved. The three-dimensional scanning diagram is shown in Figure 4, and the planar layout of the flexible structure is shown in Figure 5. Wind pressure data sampling frequency is 100 Hz. The monitoring time was from 0:00 to 12:00 on 14 July 2013, when the super typhoon Suli was weakened and landed at Yueqing City, Zhejiang Province. The maximum wind speed reached 11.59 m/s, and the wind power level reached 6 grades. Strong winds can be used as the data for the analysis of non-Gaussian properties of flexible structures under strong winds.

The measured wind pressure data includes 21 points' upper surface wind pressure $p^u(t)$ and lower surface wind pressure $p^d(t)$; the integrated wind pressure of 21 points can be obtained by differential pressure formula $\Delta p(t) = p^u(t) - p^d(t)$ as shown in Figure 6. The measured wind pressure values at 21 measurement points have different levels of intermittent large pulse values, that is, non-Gaussian characteristics. By verifying the probability density function, it was found that the wind pressure value of point #4 was too large and was obviously disturbed by noise; thence it is not suitable for analysis.

According to the records of the wind speed and wind direction measuring instruments, the horizontal wind speed and wind direction are obtained in Figures 7(a) and 7(b). In the detection period, the wind direction around the Yueqing stadium is 180° to 225°, which belongs to the southeast wind.

Table 1: Surface wind pressure detection system.

Equipment name	Model/specification	Quantity	Unit
Lightning-proof load cell CYG1721 (top surface) and mine-type differential pressure wind load sensor CYG1722 (lower surface)	CYG1721/1722-±3 KPa/accuracy class: 0.5% FS; output: 4–20 mA; power supply: 24 VDC; installation interface: Φ54 × 16 mm	124	Couple
256-channel sampler	SQCSCP-256: the system main instrument box, the linear power source, the 256-channel signal lightning protection module (must have the mine proof authentication certificate), the signal sampling conversion board, the A/D board, the connector, the industry control computer, and the observation and control software and so on; composes 256 test systems	1	/
Shielding gas-shielded waterproof cable	Shielded air-guided waterproof cable, 2-core conductor core color red, white; single-core conductor resistance is less than 94.6 ohms	50000	Meter

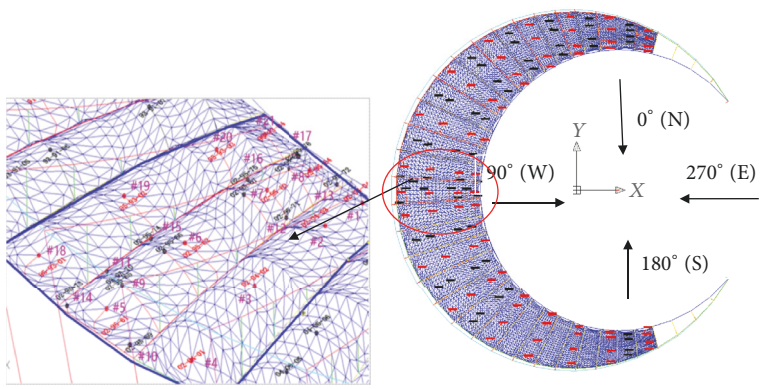

Figure 2: Flexible structure wind pressure measuring points layout.

Select T as the time interval; the mean wind speed $\overline{v}$ can be expressed as

$$\overline{v} = \frac{1}{T}\int_0^T v(t)\,dt. \tag{5}$$

In general, T takes 10 minutes as the basic time interval, but, in this study, the selected measuring time is only one hour; it is difficult to reflect the characteristics of the wind field if it takes 10 minutes as time interval, so 3 minutes are chosen as the basic time interval. The mean wind speed time history and mean wind direction time history of the basic time interval are shown in Figures 8(a) and 8(b). In the restricted observation time from 4:00 to 5:00, the total average wind speed is 4.55 m/s, and the maximum average wind speed at 3 min is 5.86 m/s.

3.2. Rigid Structure Field Measurement. In order to analyze the non-Gaussian characteristics of wind pressure acting on the rigid structural surface, a rectangular masonry structure (length: 5.5 m; width: 3.6 m; height: 1.85 m) on the roof of an office building located in East China Jiaotong University was chosen as the test object, and the field measurement of wind pressure was implemented, respectively, on 23 November 2012 and 1 March 2013.

The first scheme of rigid structure (R1) as shown in Figure 9 was carried out on 23 November 2012. The weather of the day was northeaster and wind force scale was 3~4. The second scheme of rigid structure (R2) as displayed in Figure 8 was implemented on 1 March 2013. On the day, the blue warning signal of a gale, norther with wind force scale of 7~8, was released

R1 was arranged to test the wind pressure on the corner of the masonry. In this scheme, the pressure sensors from #1 to #5 were fixed on the metope AB of the rectangular structure as shown in Figure 9(b). And other sensors from #6 to #10 were installed on the metope AD. The vertical interval of these sensors on every wall is 21 cm, and the horizontal distances to corner A are 23 cm. In addition, the perpendicular distances from the masonry top edge to the pressure sensors #1 and #6 are 18 cm.

R2 was designed to measure the wind pressure around the structure. In the same horizontal plane, as indicated in Figure 10(b), #1 to #3 and #7 to #9 sensors fixed on AB and CD metope, respectively, were set using the interval of 2.45 m, while #4 to #6 and #10 to #12 sensors on BC and DA metope, respectively, were arranged by the interval of 1.5 m. All the 12 wind pressure sensors are 39 cm away from the top edge of the structure. #1 and #12, #3 and #4, #6 and #7, and #9 and #10 sensors, respectively, have a horizontal distance of 30 cm to corners A, B, C, and D of the structure.

A kind of pressure sensor, CYG1513T, has been developed to measure wind pressures by the way of attaching to

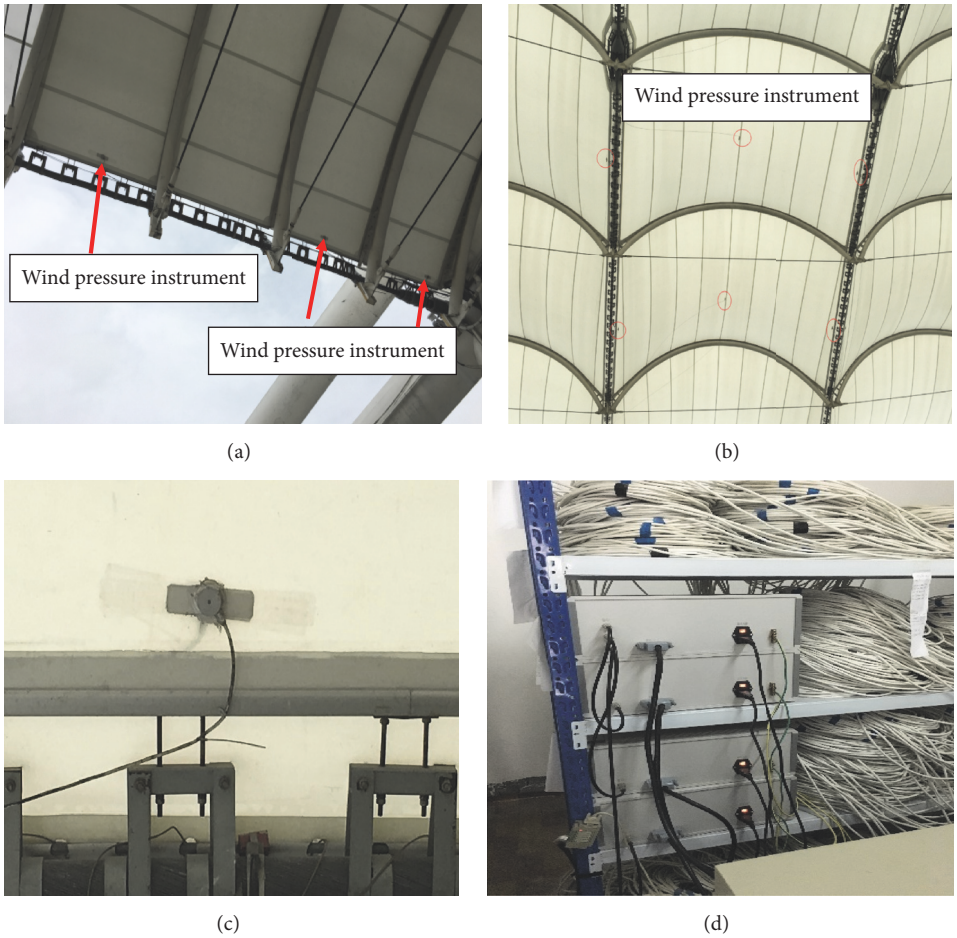

Figure 3: Layout of field wind pressure instrument. (a) Arrangement of side span of wind pressure instrument. (b) Arrangement of middle span of wind pressure instrument. (c) Wind pressure instrument. (d) Sampling channels and cables.

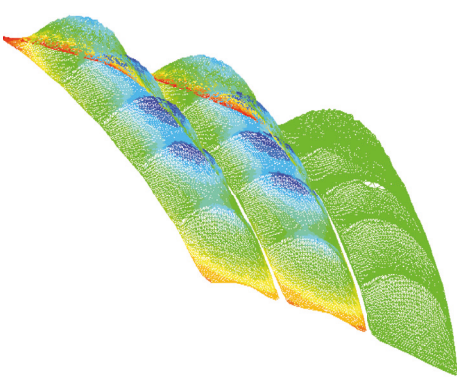

Figure 4: 3D scanning of the middle three pieces of film.

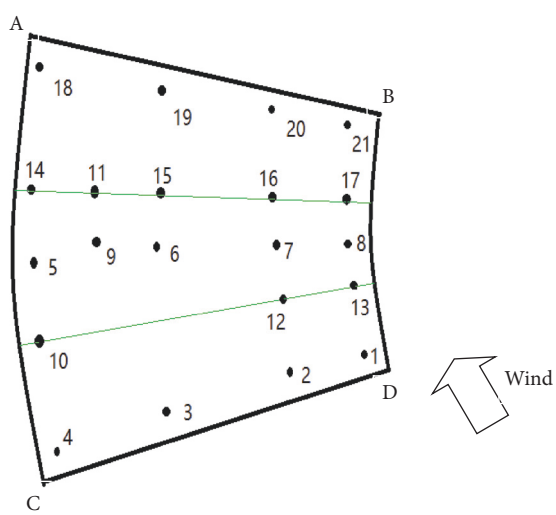

Figure 5: Planar layout of the flexible structure.

the building surface, and the field measurement adopting CYG1513T to test the wind pressure on a building structure has been carried out in the literature [35]. Then, the kind of pressure sensor was improved by the developers as the type CYG1721T becomes thinner and smaller. In the two field measurements, the improved sensor, CYG1721T, is adopted to measure wind pressures through attaching to the building surface. The sampling frequency of 20 Hz was

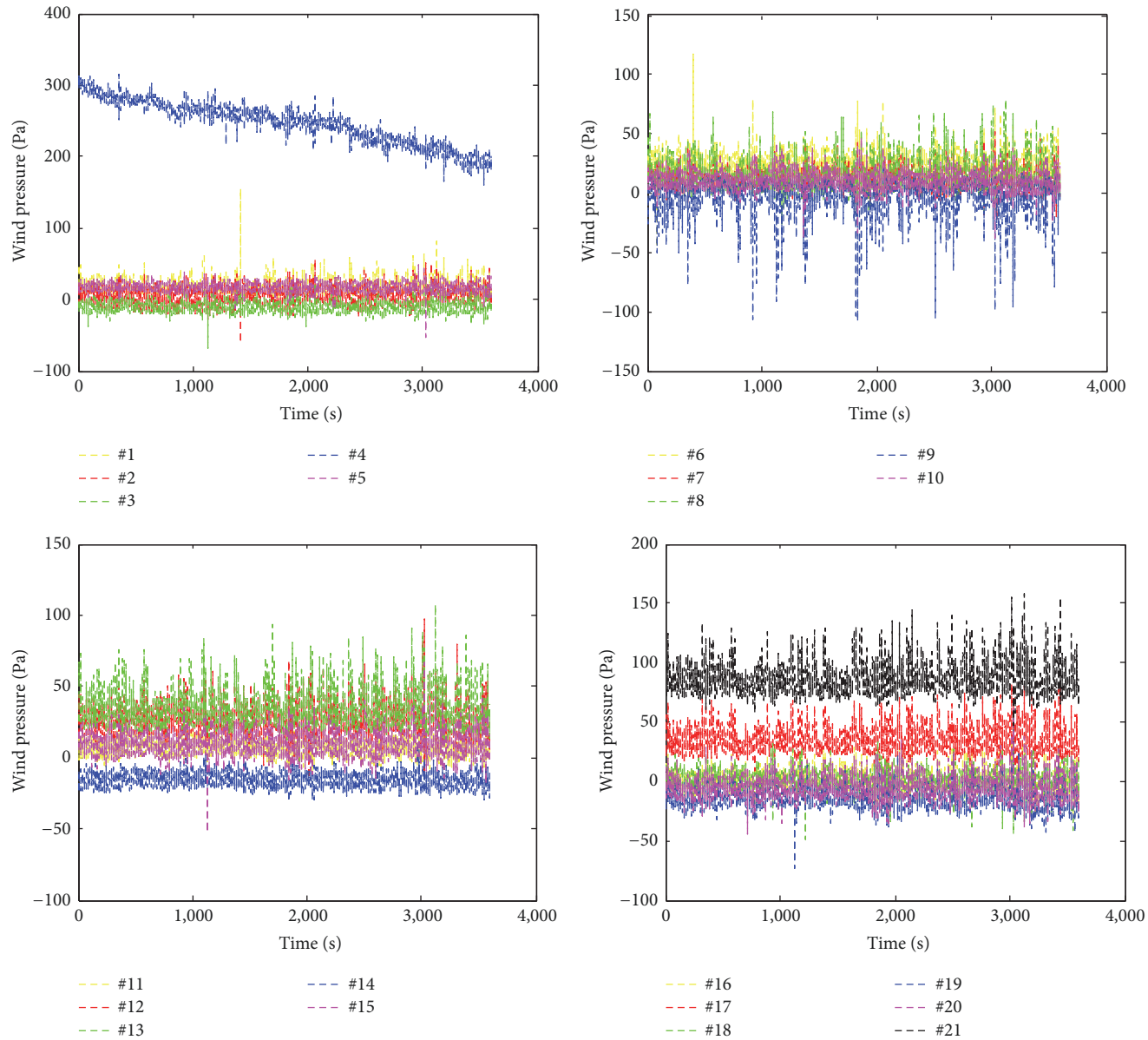

Figure 6: The measured value of the wind pressure on the 21 measuring points.

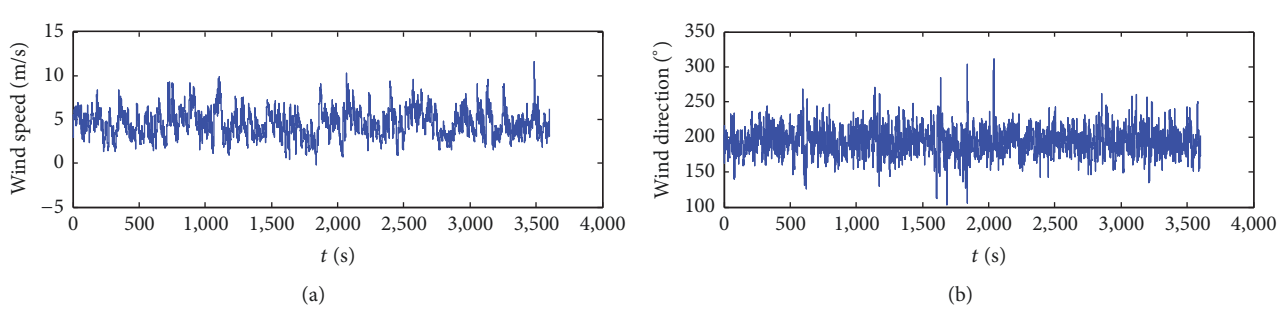

Figure 7: Time series of horizontal wind speed and wind direction. (a) Time series of horizontal wind speed. (b) Time series of wind direction.

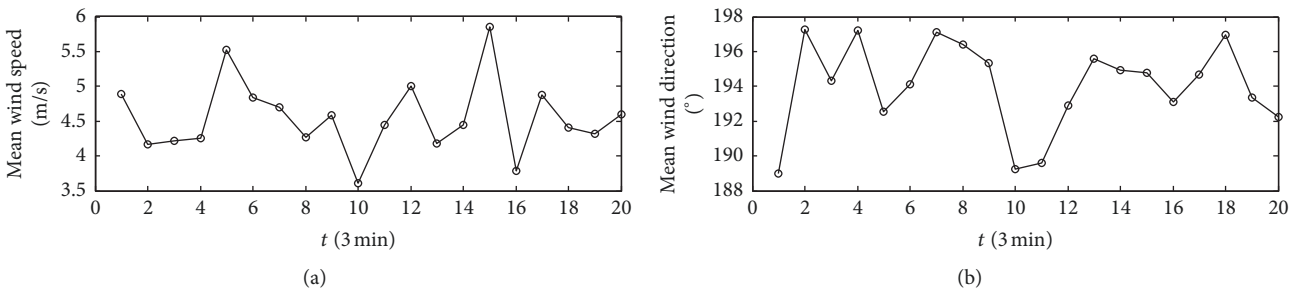

Figure 8: Mean wind speed and mean wind direction. (a) Mean wind speed (3 min). (b) Mean wind direction (3 min).

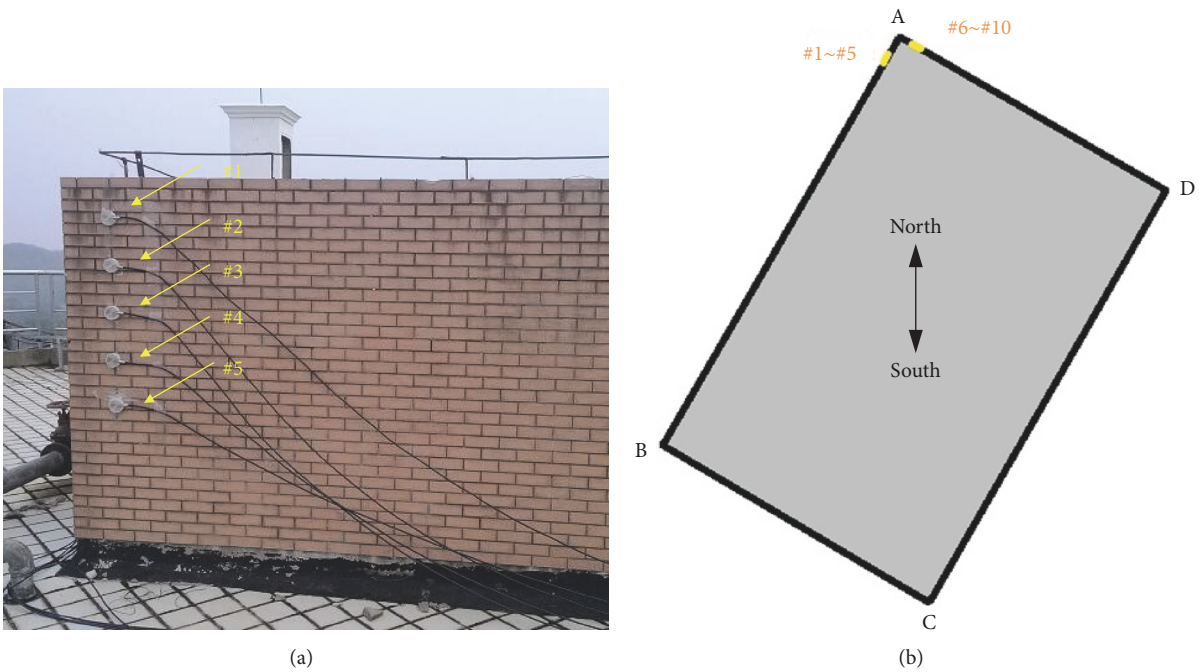

Figure 9: The first scheme of rigid structure field measurement. (a) Site layout. (b) Plane layout of the rigid structure.

set in the two field measurements, and the low-pass filter of 10 Hz was adopted to improve the wind pressure data collection.

In the process of R1, it is northeaster on that day. Therefore, DA metope was located in the windward side; AB metope belonged to the nonwindward side. On the day of the R2, it is norther. So, AB and DA walls were situated in the windward side, while BC and CD walls were seated in the nonwindward side. The measured wind pressures of two tests are shown in Figures 11 and 12. Apparently, all of them possess the sharp intermittent pulse, which shows the non-Gaussian characteristics. It can be observed from Figure 11 that the skewness of wind pressures on the windward side is not very obvious; namely, the distribution of wind pressure is symmetry, while wind pressures on the nonwindward side reveal marked skewness. Likewise, in Figure 12, the wind pressures of the nonwindward sides BC and CD are more skew than those of the windward sides AB and DA. Therefore, it can be determined that the nonwindward side and the windward side have different degrees of non-Gaussian wind pressures, and the skewness of wind pressures on the nonwindward side is more obvious.

However, in order to further research the features of the non-Gaussian wind pressures for rigid structure and flexible structure, it is necessary to analyze the probability distribution function (PDF), high-order statistical characteristic, correlation, and power spectral density (PSD).

4. Results and Discussions

4.1. PDF of the Non-Gaussian Wind Pressures. The probability density function (PDF) describes the numerical distribution characteristics of random variables, and it is an important basis for studying the non-Gaussian properties of wind pressure. The PDF is calculated for the wind pressure values of field measurement programs and compared with the

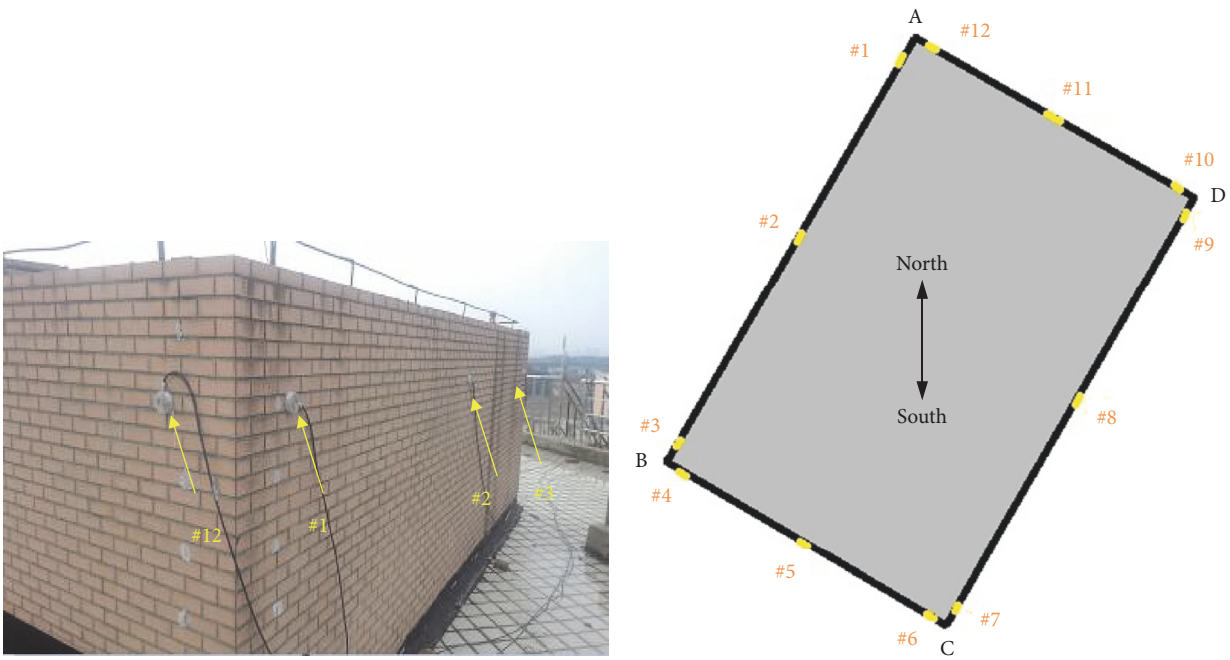

(a) (b)

Figure 10: The second scheme of rigid structure field measurement. (a) Site layout. (b) Plane layout of the rigid structure.

Table 2: Corresponding measuring points of the windward side and leeward side in field measurement programs.

Field measurement program	Windward side	Leeward side
Flexible structure	BC side: #1, #13, #8, #17, #21	AD side: #10, #5, #14, #18
The first scheme of rigid structure (R1)	AD side: #6, #7, #8, #9, #10	AB side: #1, #2, #3, #4, #5
The second scheme of rigid structure (R2)	AB side: #1, #2, #3 AD side: #10, #11, #12	BC side: #4, #5, #6 CD side: #7, #8, #9

Gaussian-type distribution, respectively. The MATLAB code can be used to calculate PDF for the data of each measuring pressure point (e.g., point 10):

```
[mu, sigma] = normfit(point 10)
[f,xi]=ksdensity(point 10);plot(xi,f,'.');
hold on;
y=-50:0.1:50;dd=normpdf(y,mu,sigma);
plot(y,dd,'r-').
```

As shown in Figures 13, 14, and 15, all the PDFs of the fluctuating wind pressures have some deviation from the Gaussian distribution. Namely, all the measured wind pressures show different degrees of non-Gaussian distribution. The PDFs of the measured wind pressures at different locations of the flexible structure roof are summarized in Figure 13, in which Figure 13(a) is the PDF of the wind pressure on AD side measuring points, Figure 13(c) shows the PDF of the wind pressure on BC side measuring points, and the measuring points picked in Figure 13(b) are inside the membrane. The corresponding measuring points of the windward side and leeward side in field measurement programs can be seen in Table 2. The PDF of the wind pressure on AD side, as the leeward side, shows a property that approaches the Gaussian distribution, and the same conclusion can be found in the wind pressure PDF of the measuring points inside the membrane. Figure 13(c) reveals that the wind pressure on BC side, which is the windward side, has obvious non-Gaussian properties with positive skewness and high kurtosis. In Figure 14, the PDFs of the fluctuating wind pressures on the leeward side are markedly asymmetrical, while the PDFs on the windward side are nearly symmetrical. However, both the leeward side and the windward side have high kurtosis of PDF. In addition, it is not obvious for the difference among the PDFs of wind pressures acting on the vertical measuring points of the same wall, and it may indicate that the non-Gaussian wind pressures of the vertical testing points have good correlations. In Figure 15, it can also be found that the leeward sides have markedly asymmetrical PDFs while the windward sides possess nearly symmetrical PDFs and that all the PDFs are with high kurtosis. Moreover, for the fluctuating wind pressures on the horizontal measuring points of the same metope, the similar PDFs may betoken that these non-Gaussian wind pressures are correlated. In conclusion, from the probability density function, the roof of flexible structure and the surface of rigid structure have a similarity that both of them show softening non-Gaussian characteristic with kurtosis higher than 3. However, the difference between them is shown as the roof of flexible structure shows strong non-Gaussian property

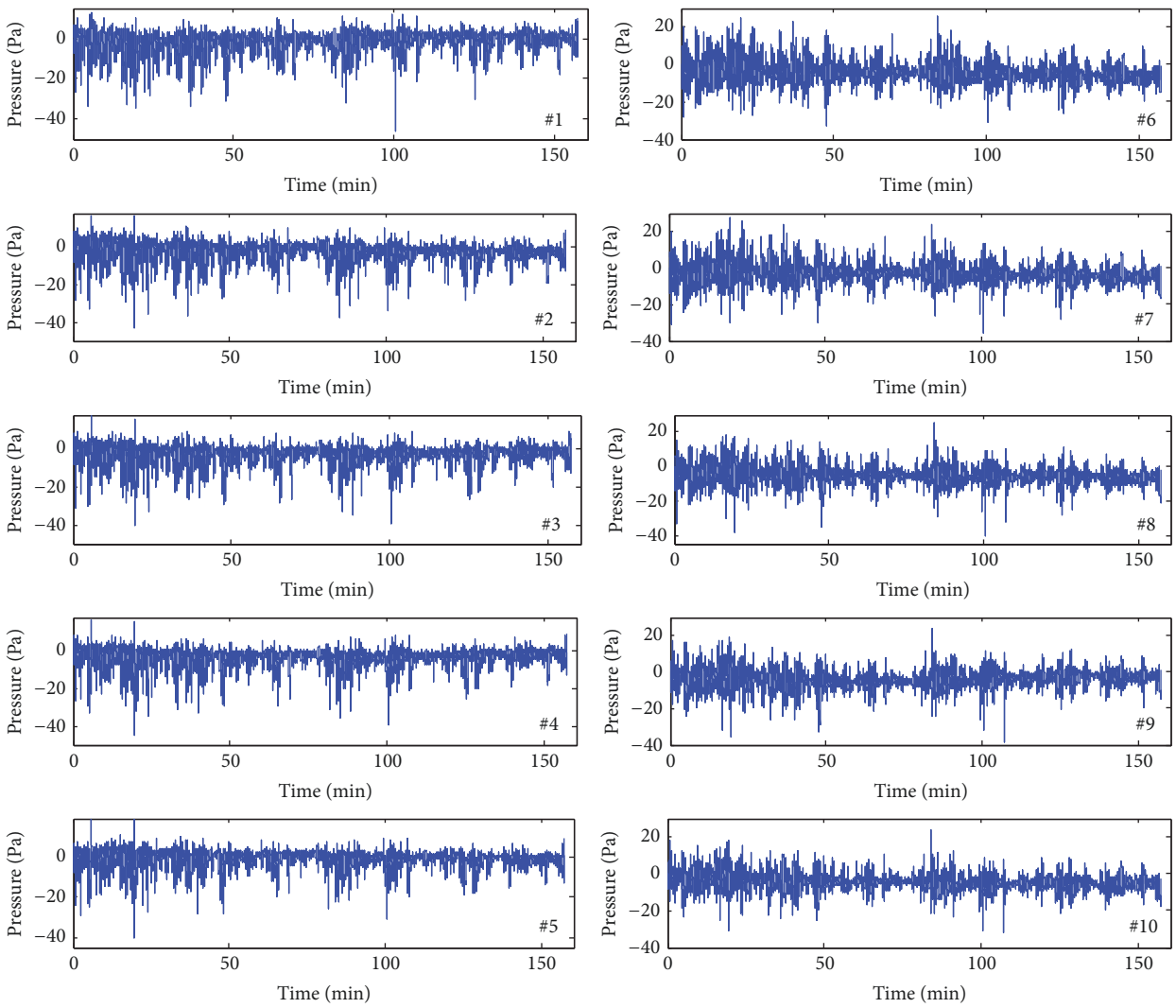

Figure 11: Time history of the measured wind pressures (R1).

in the windward side, which is also found by Kumar and Stathopoulos [7], while the surface of rigid structure shows non-Gaussian property mainly in the leeward. The latter conclusion can be explained as follows: by the comprehensive effect of the separated flow and wake, the surface of rigid structure reflects negative skewness and large kurtosis (higher than 3) in the leeward side; this phenomenon has also been found by Han and Gu [15].

4.2. High-Order Statistic Characteristic of the Non-Gaussian Wind Pressures. For the non-Gaussian wind pressures, it is significant to master the high-order statistic characteristics, such as skewness and kurtosis. In order to analyze the high-order statistic characteristics, the measured wind pressures of rigid structure are divided into many segments in ten-minute interval, while the measured wind pressures of flexible structure are divided into many segments in three-minute interval on account of the short sampling time. Based on these segments of the measured wind pressures, the relationships between skewness and kurtosis are displayed in Figures 16, 17, and 18. It is known that the skewness and kurtosis of the Gaussian wind pressures are 0 and 3, respectively. However, it can be seen from the three figures that there are some deviations in the skewness and kurtosis between the measured wind pressures and the Gaussian wind pressure.

By observing Figure 16(a), the leeward side's wind pressures show weak non-Gaussian property with the kurtosis distributing mainly in the interval $[2, 6]$ and the skewness is in the interval $[-0.5, 1.0]$. Figures 16(b) and 16(c) show the skewness and kurtosis of the fluctuating wind pressures on CD side and AB side which are parallel to the wind direction, and the distribution of skewness and kurtosis is similar to that in Figure 16(a). The fluctuating wind pressures of the windward (BC side) measuring points in Figure 16(d) show the strong non-Gaussian property with the kurtosis distributing mainly in the interval $[3, 7]$ and the skewness is in the interval $[0.5, 2.0]$. In Figure 17, it can be found that the fluctuating wind pressures of the nonwindward measuring points #1~#5 show negative bias, while those of the windward

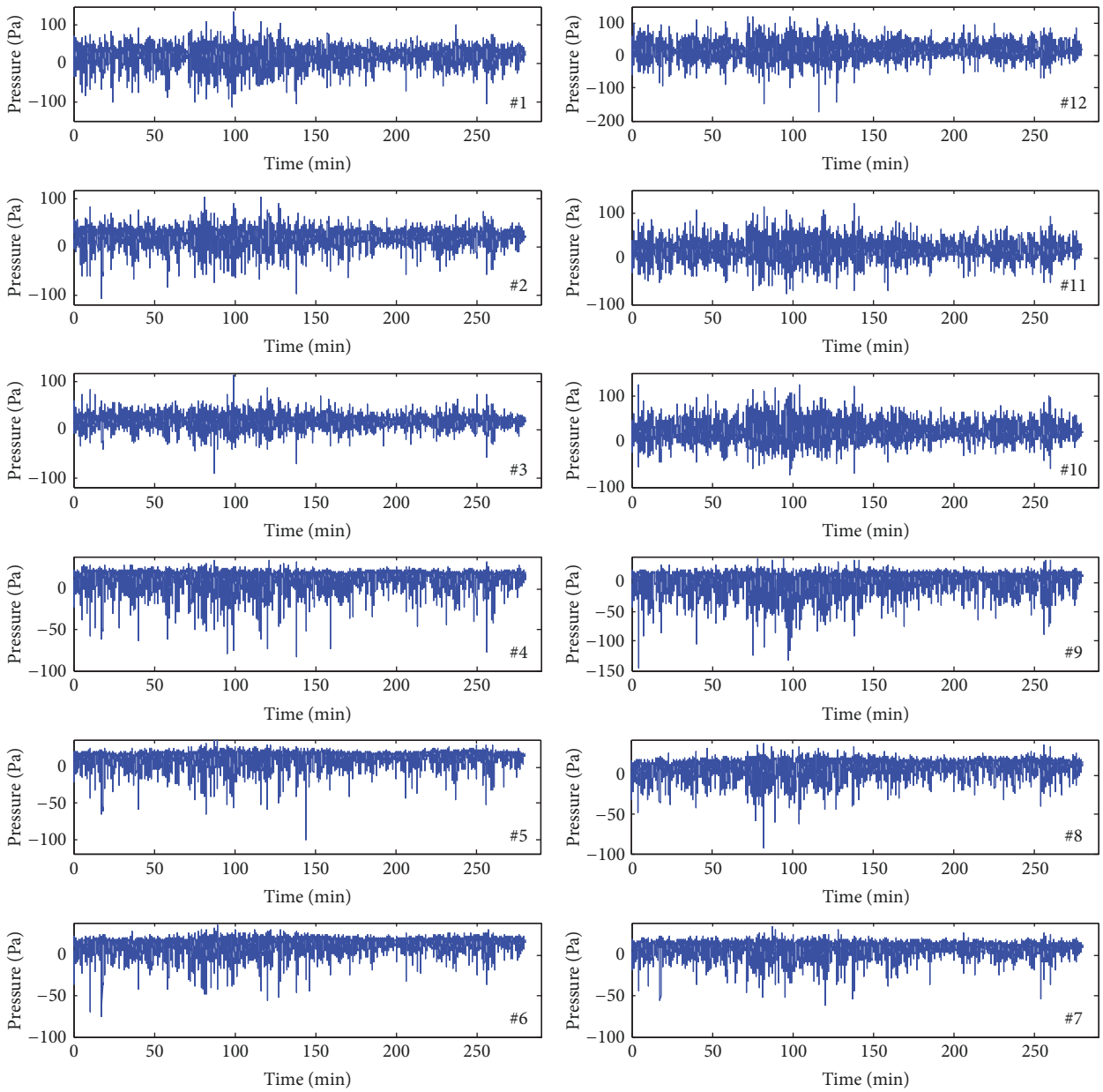

Figure 12: Time history of the measured wind pressures (R2).

measuring points #6~#10 display positive or negative bias. Meanwhile, the kurtosis distributes mainly in the interval $[3, 9]$ when the skewness is in the interval $[-1.0, 1.0]$. In Figure 18, these similar characteristics can be also found for the non-Gaussian wind pressures measured in R2. Besides, in these three figures, it can be seen that the kurtosis rapidly increases along with the increase of the absolute value of the skewness.

4.3. The Correlation of the Non-Gaussian Wind Pressures

4.3.1. The Correlation of the Wind Pressures between Measuring Points. A correlation function is a function that gives the statistical correlation between random variables; it can be classified into autocorrelation function and cross-correlation functions. The correlation of the non-Gaussian wind pressures measured in R1 is displayed in Figure 19. From this figure, it can be determined that the correlation decays very quickly to zero after a really short delay time, and the correlation weakens along with the increase of spacing. In addition, the correlation of the non-Gaussian wind pressures on the DA metope is stronger than that on the AB metope, indicating that the correlation of the windward is better than that of the leeward. And, on the vertical measuring points of the same metope, the correlation decreases slowly, which is the reason why the spacing of measuring point is smaller and the wind simultaneously arrives at the vertical measuring point (namely, no existence of the phase angle).

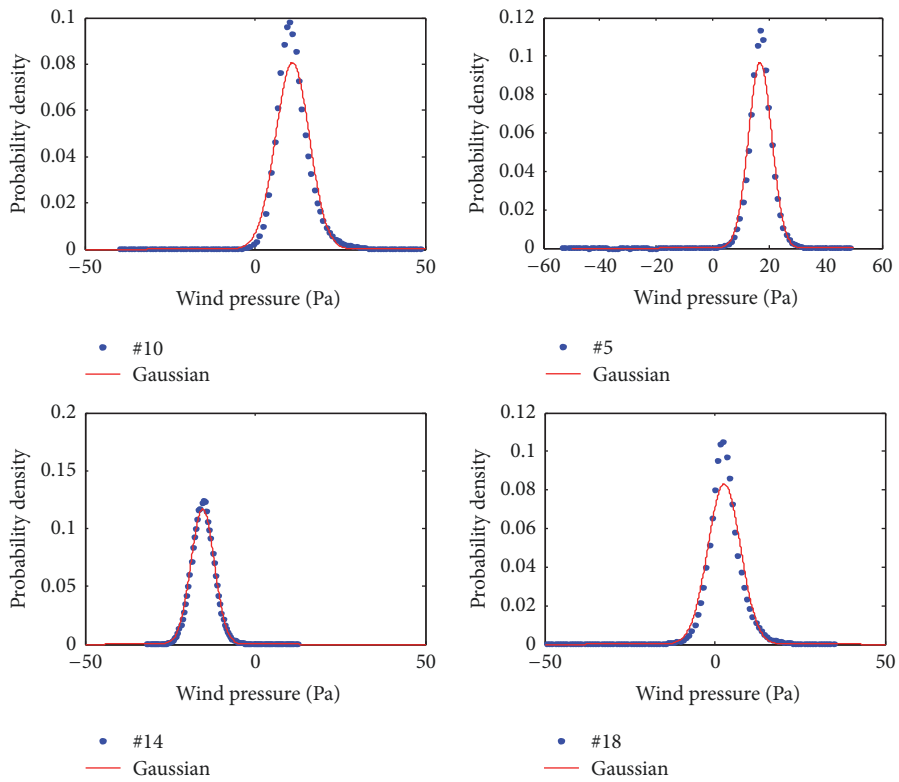

(a)

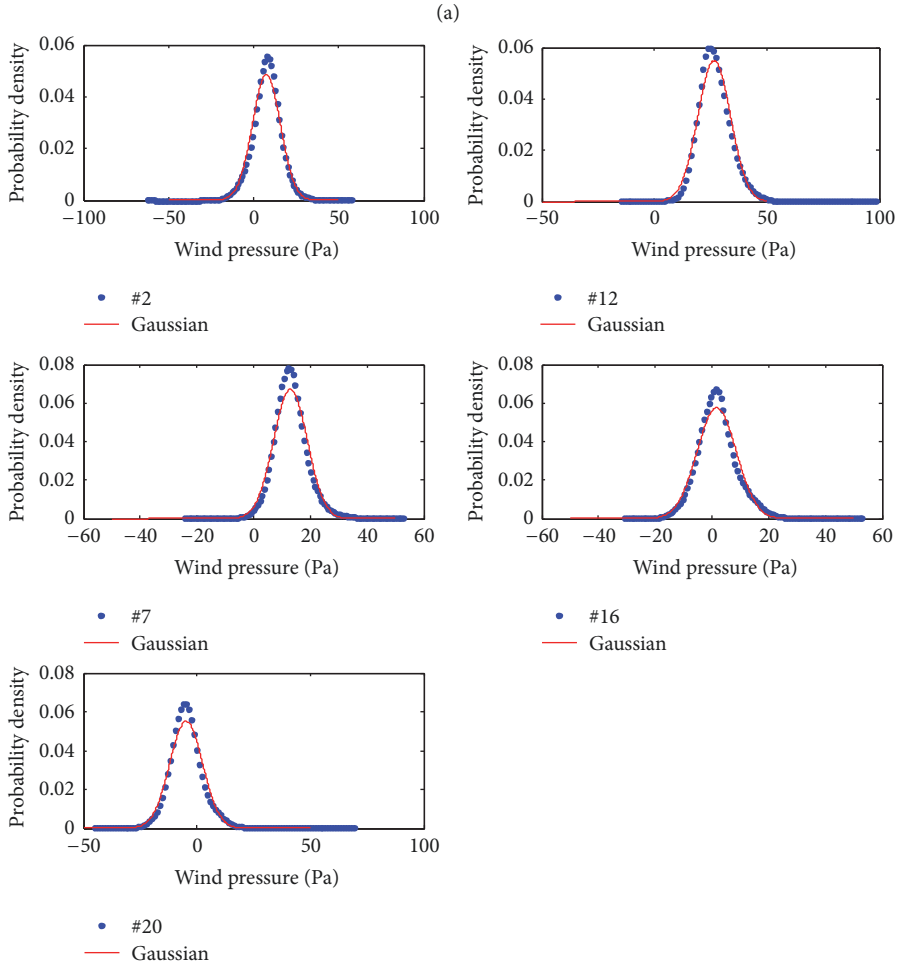

(b)

Figure 13: Continued.

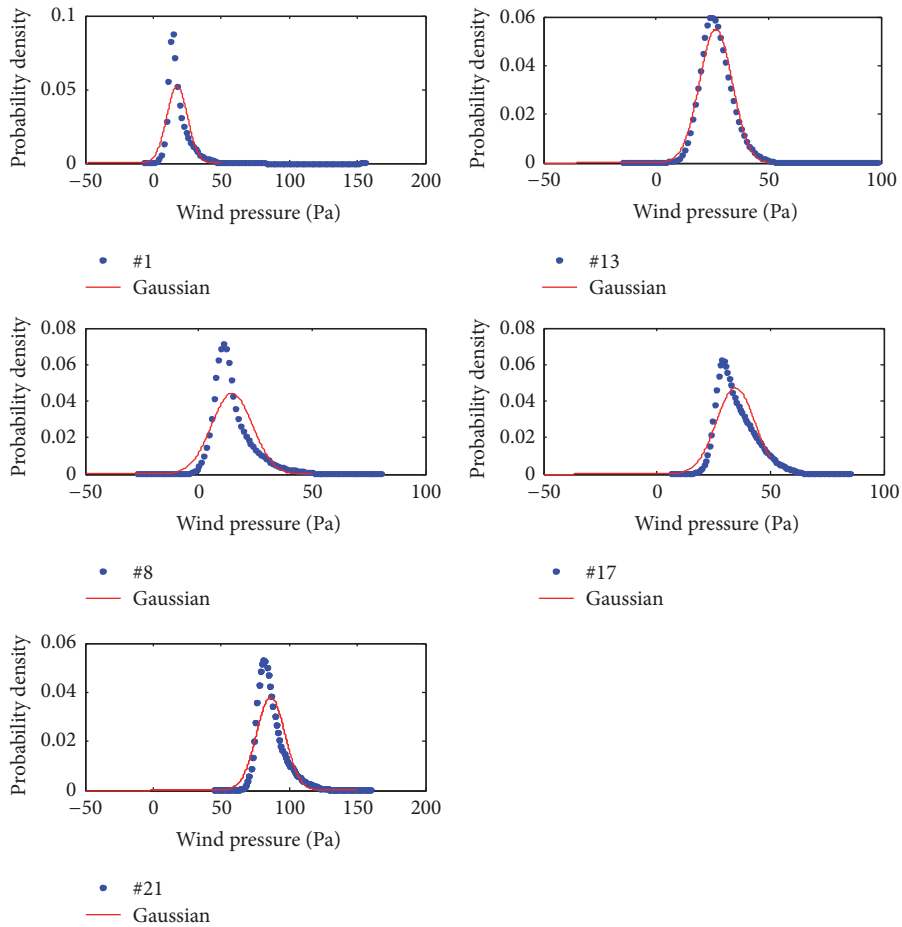

(c)

Figure 13: The PDF of the measured wind pressures (the flexible structure). (a) AD side measuring points. (b) Selected measuring points inside the membrane. (c) BC side measuring points.

This may be the reason why, for the vertical measuring points of the same metope, the PDFs of the non-Gaussian wind pressures have no obvious difference as shown in Figure 14.

In R2, between these horizontal measuring points, the correlation of non-Gaussian fluctuating wind pressure also conforms to the rule that the correlation decreases with the increase of spacing as shown in Figure 20. Clearly, the correlation also decays very quickly. And the peak value of the correlation has an obvious time shifting, indicating that there exists the phase difference between the fluctuating wind pressures of these horizontal measuring points. The reason why the phase angle exists is that there is a definite angle between the same plane of the horizontal measuring points and the cross section of the wind and that the wind cannot reach each horizontal measuring point at the same time. Furthermore, the angle can influence the perpendicular distance from the horizontal measuring point to the cross section of the wind, so that it affects the cross-correlation of the fluctuating wind pressures between these measuring points. In Figure 20, it can be also found that the correlation of the non-Gaussian wind pressures on the windward metope is stronger than that on the leeward metope.

The analysis of Figure 21 reveals the correlations of the measured non-Gaussian wind pressures for the flexible structure in different arrangement directions, which have a significant difference from the rigid structure. Figures 21(a), 21(b), and 21(c) show the correlation of the measured wind pressures for the AD side points, the AB side points, and the BC side points, respectively. Compared with Figures 19 and 20, the same conclusion can be obtained that the correlation of wind pressures between measuring points on the windward side is stronger than that on the leeward side, while the differences are obviously shown as follows: first, #18~#14 in Figure 21(a) and #21~#20 and #21~#19 in Figure 21(b) show negative correlations, respectively. Owing to the complex wave structure of the membrane structure, the wind pressures of some measuring points like #9, #19, and #14 reveal negative values as shown in Figure 6, simultaneously leading to the negative correlation of the wind pressure in some areas. Second, the maximum of the cross-correlation function or the minimum of the negative correlation indicates the point

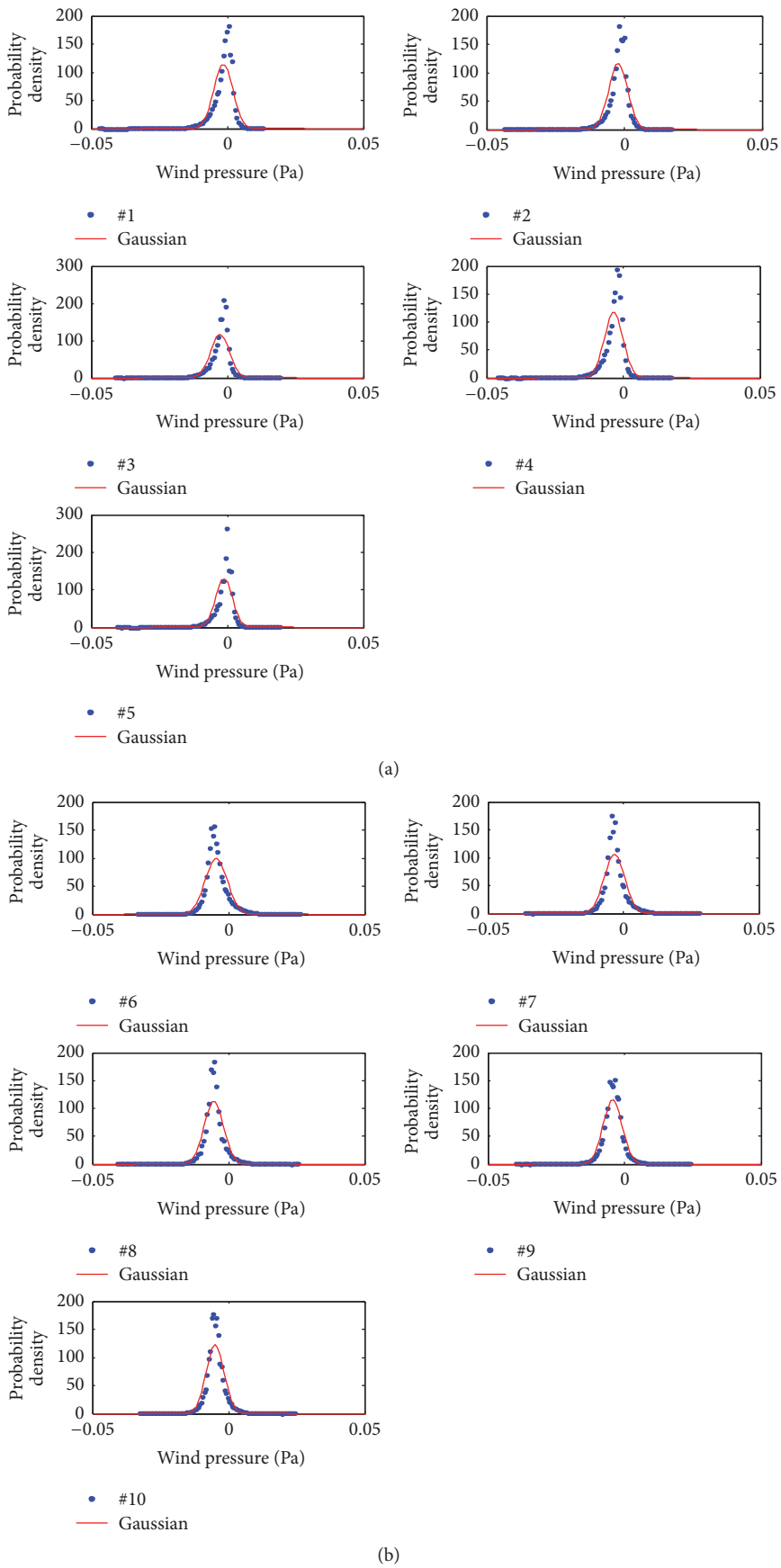

Figure 14: The PDF of the measured wind pressures (R1). (a) AB side measuring points. (b) AD side measuring points.

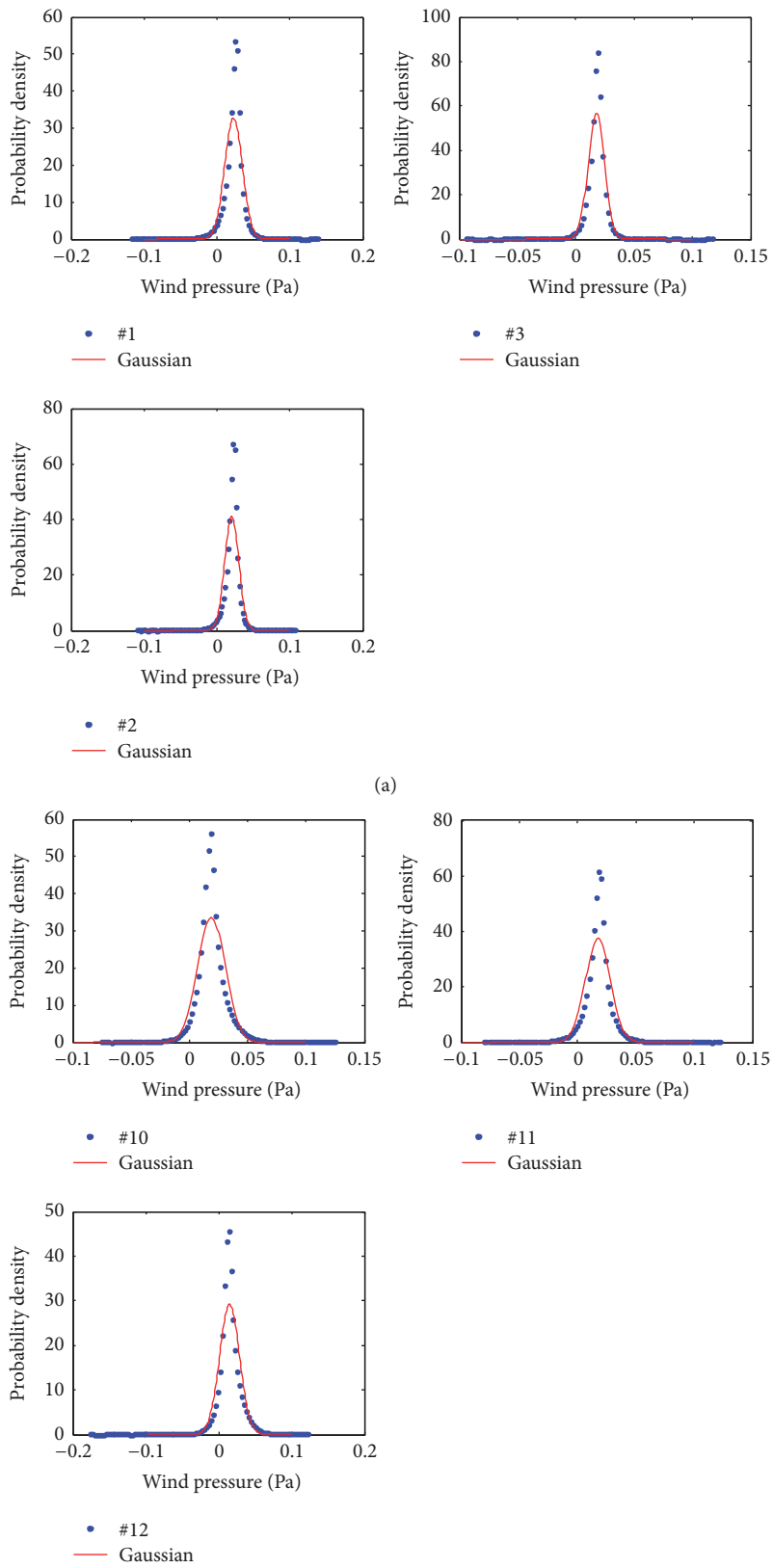

Figure 15: Continued.

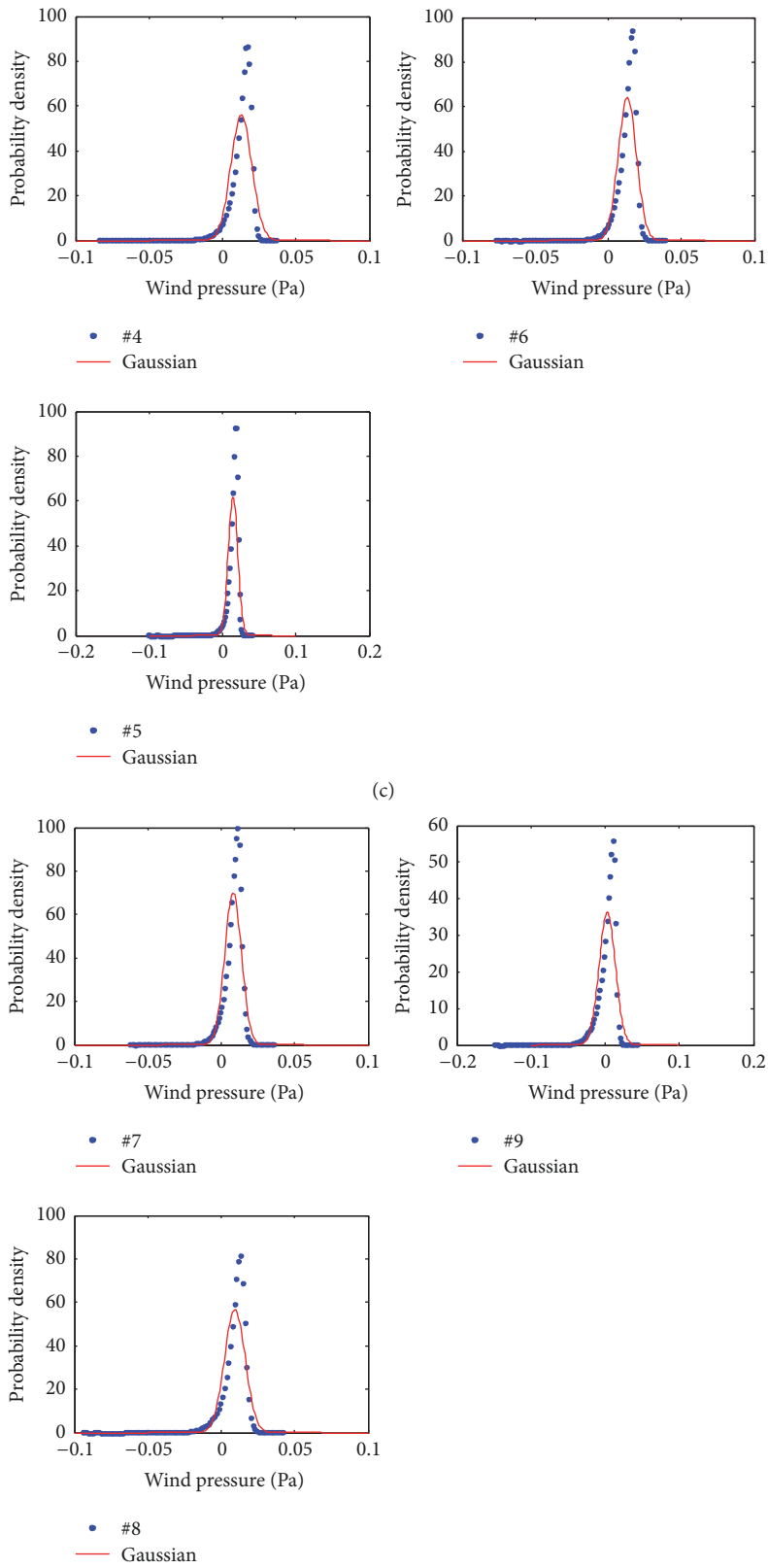

Figure 15: The PDF of the measured wind pressures (R2). (a) AB side measuring points. (b) AD side measuring points. (c) BC side measuring points. (d) CD side measuring points.

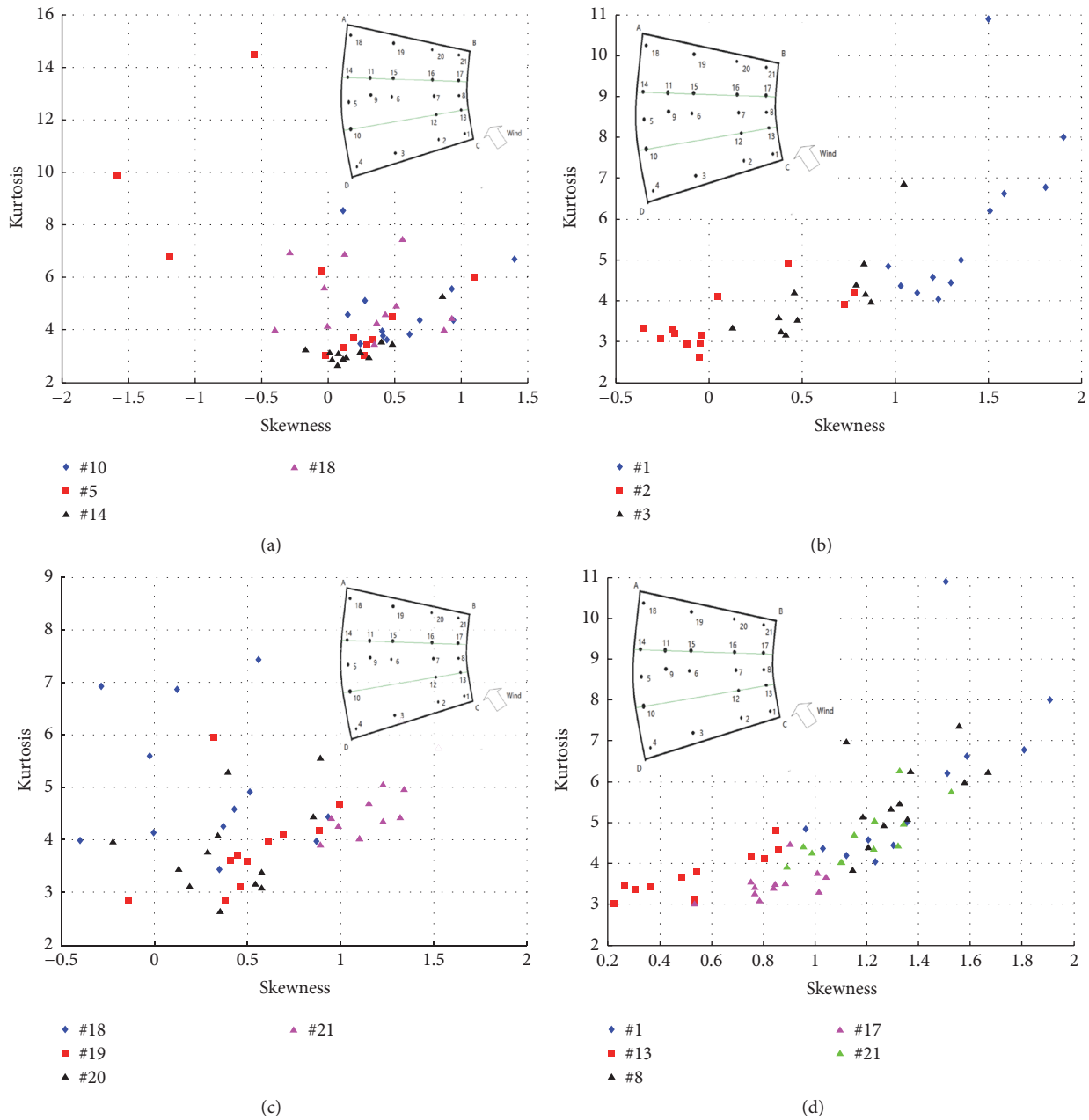

Figure 16: The relationship between skewness and kurtosis of the fluctuating wind pressures (the flexible structure). (a) AD side; (b) CD side; (c) AB side; and (d) BC side.

in time where the signals are best aligned; that is, the time delay between the two signals is determined by the argument of the extreme value [38]; Figures 21(a) and 21(b) show the obvious delay time between the wind pressures of the measuring points due to the long distance and the changing wind direction. However, the delay time between the wind pressures of the measuring points in Figure 21(c) is relatively close to zero, which means that the wind simultaneously arrived at the BC side measuring points.

4.3.2. The Correlation of the Wind Pressures on Upper and Lower Surface of Flexible Structure. In order to further study the special relationship between the wind pressures of the flexible structure, the correlation analysis of the measured wind pressure data of the upper and lower surface of the membrane structure is carried out.

For large-span membrane structures, the direction of the wind pressure coincides with the direction of the upper surface wind pressure. The wind pressure coefficient $\mathrm{Cp}(t)$ of the measuring point can be expressed as

$$\mathrm{Cp}(t) = \frac{p^u(t) - p^d(t)}{1/2\rho U^2} = \mathrm{Cp}u(t) - \mathrm{Cp}d(t), \quad (6)$$

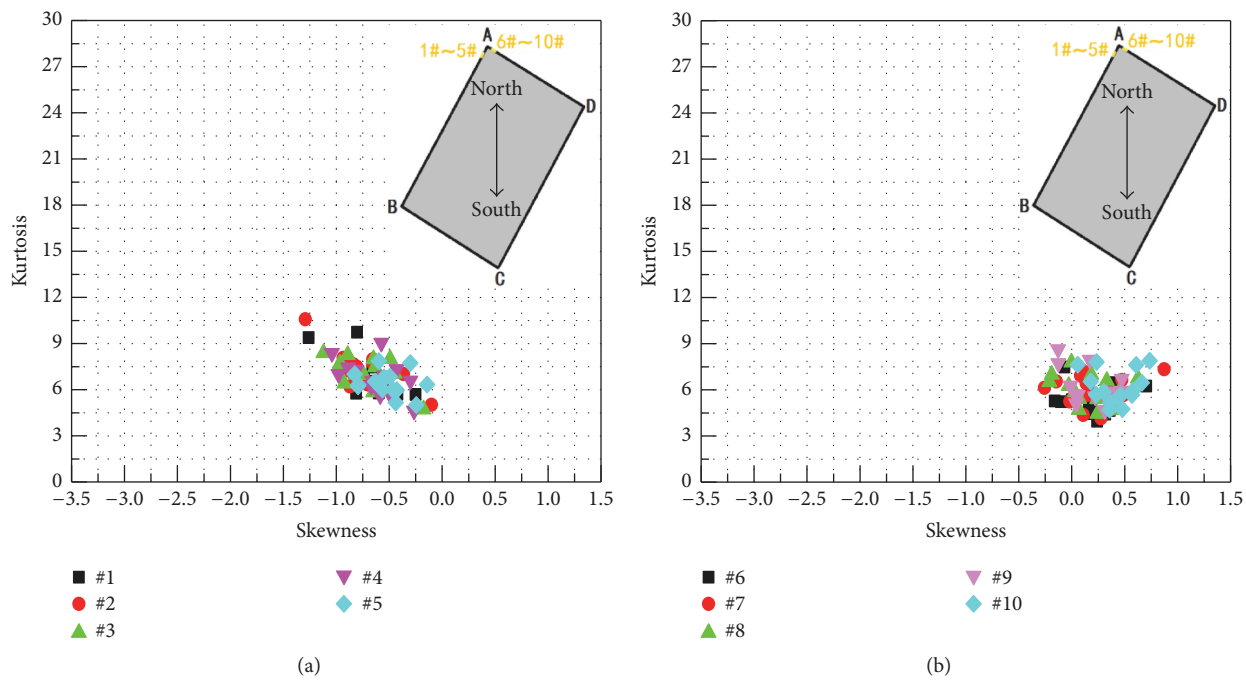

FIGURE 17: The relationship between skewness and kurtosis of the fluctuating wind pressures (R1).

where $p^u(t)$ is the wind pressure measured on the upper surface of the measuring point and $p^d(t)$ is the lower surface wind pressure; $\mathrm{Cp}u(t)$ and $\mathrm{Cp}d(t)$ are the wind pressure coefficients of the upper and lower surfaces, respectively.

The wind pressure root mean square coefficient $\mathrm{Cp}_{\mathrm{rms}}$ can be obtained by computing the root mean square p_{rms} of the wind pressure:

$$\mathrm{Cp}_{\mathrm{rms}} = \frac{p_{\mathrm{rms}}}{1/2\rho U^2}. \tag{7}$$

According to the nature of the multidimensional random variable [39], (7) can be expressed as

$$\mathrm{Cp}_{\mathrm{rms}}(t) = \sqrt{\mathrm{Cp}^2_{\mathrm{rms}\cdot u}(t) + \mathrm{Cp}^2_{\mathrm{rms}\cdot d}(t) - 2\gamma_{ud}\mathrm{Cp}_{\mathrm{rms}\cdot u}(t)\,\mathrm{Cp}_{\mathrm{rms}\cdot d}(t)}, \tag{8}$$

where $\mathrm{Cp}_{\mathrm{rms}\cdot u}(t)$ and $\mathrm{Cp}_{\mathrm{rms}\cdot d}(t)$ are the upper and lower surface of the wind pressure root mean square coefficient, respectively. γ_{ud} is the correlation coefficient of the upper and lower surface wind pressure, which is defined by

$$\gamma_{ud} = \frac{E\left[\mathrm{Cp}u(t)\,\mathrm{Cp}d(t)\right] - E\left[\mathrm{Cp}u(t)\right]E\left[\mathrm{Cp}d(t)\right]}{\mathrm{Cp}_{\mathrm{rms}\cdot u}(t)\,\mathrm{Cp}_{\mathrm{rms}\cdot d}(t)}. \tag{9}$$

In order to facilitate the calculation, (8) is employed:

$$\gamma_{ud} = \frac{\mathrm{Cp}^2_{\mathrm{rms}\cdot u}(t) + \mathrm{Cp}^2_{\mathrm{rms}\cdot d}(t) - \mathrm{Cp}^2_{\mathrm{rms}}(t)}{2\mathrm{Cp}_{\mathrm{rms}\cdot u}(t)\,\mathrm{Cp}_{\mathrm{rms}\cdot d}(t)}. \tag{10}$$

If the upper and lower surface wind pressure signals are not related to each other, that is, $\gamma_{ud} \approx 0$, the wind pressure root mean square coefficient $\mathrm{Cp}_{\mathrm{rms}}$ can be approximated as

$$\widetilde{\mathrm{C}}\mathrm{p}_{\mathrm{rms}}(t) = \sqrt{\mathrm{Cp}^2_{\mathrm{rms}\cdot u}(t) + \mathrm{Cp}^2_{\mathrm{rms}\cdot d}(t)}. \tag{11}$$

Comparing (8) and Eq. (11), if there is a strong correlation between the upper and lower surface wind pressure signals, the approximate calculation of (11) will produce a large error.

When $\gamma_{ud} > 0$ and $\widetilde{\mathrm{C}}\mathrm{p}_{\mathrm{rms}}(t) > \mathrm{Cp}_{\mathrm{rms}}$, the designed wind load is conservative; when $\gamma_{ud} < 0$ and $\widetilde{\mathrm{C}}\mathrm{p}_{\mathrm{rms}}(t) < \mathrm{Cp}_{\mathrm{rms}}$, the designed wind load is dangerous.

Figure 22(a) is the time-history analysis of the correlation of the wind pressures on upper and lower surface of the measuring point #1 by taking 3-minute averages, and it reveals that the correlation coefficient does not change with time obviously. Therefore, the average of all 21 measurement points can be obtained in the same way, and the correlation coefficient histogram of all 21 measurement points can be obtained as shown in Figure 22(b).

By observing Figure 22(b), the measuring points with negative correlation coefficients are scattered as Figure 23. It can be found that most of these points are close to the BC side of the membrane, which is the windward side, and the correlation coefficient of the measurement points in the leeward side of the membrane is mostly positive. This phenomenon can be explained in physical sense. During the course of strong wind, due to the existence of the tilt angle of the membrane structure (AD surface is high; BC surface is low), the upper surface of the windward side edge of the membrane is under great pressure, and the lower surface of these area is subject to great suction due to Bernoulli effect, leading to the negative correlation of these areas, while

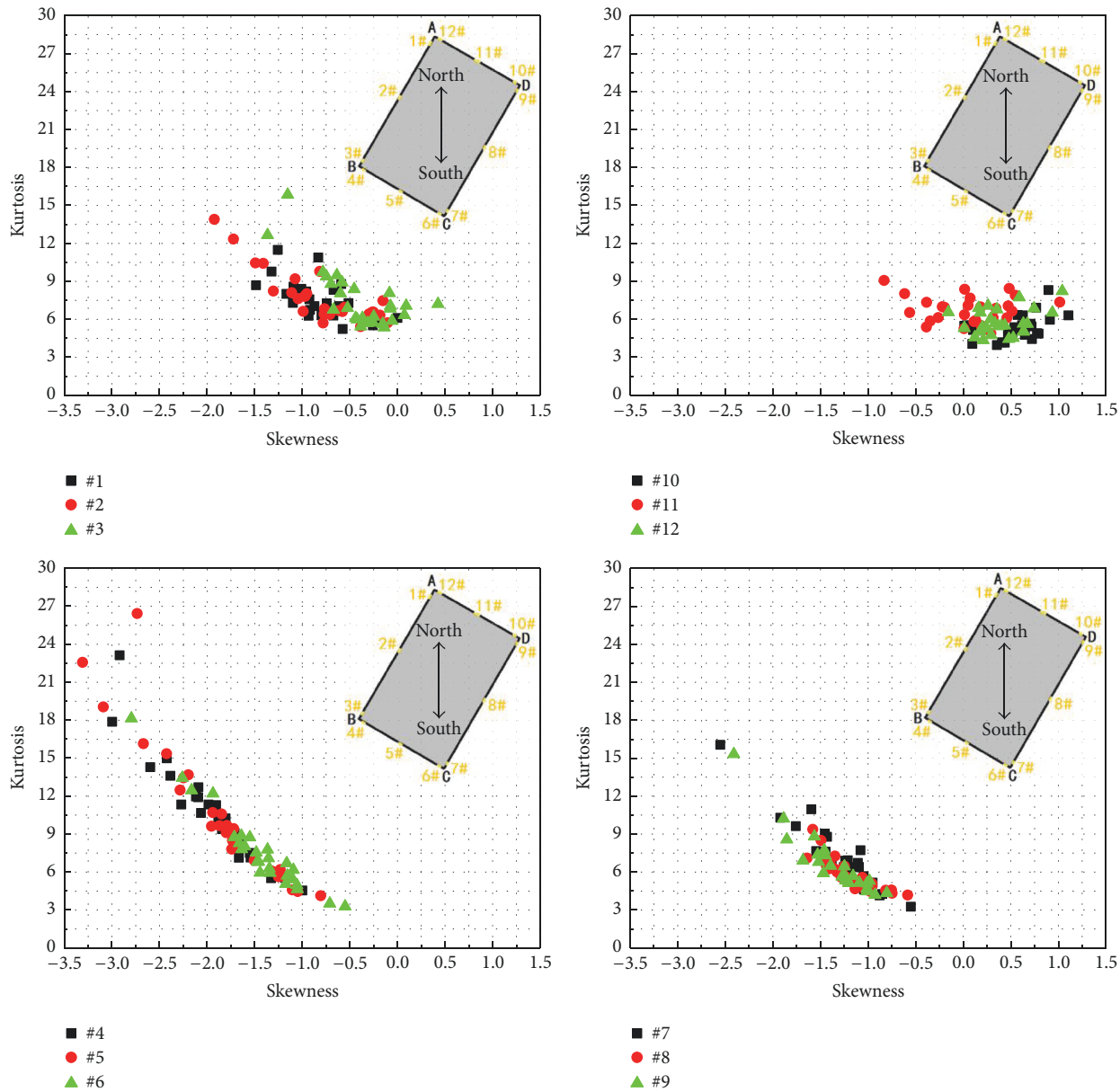

Figure 18: The relationship between skewness and kurtosis of the fluctuating wind pressures (R2).

other regional wind pressures reached a relative balance, belonging to the positive correlation area. For large-span membrane structures, this type of negative correlation causes a bigger wind pressure root mean square coefficient Cp_{rms}. Therefore, when considering the structural wind load design value, the negative correlation area of wind pressure should be checked.

4.4. PSD of the Non-Gaussian Wind Pressures. Power spectral density (PSD) estimation methods mainly include classical spectral estimation and modern power spectral estimation, namely, the parameter spectral estimation method. The process is estimating parameter model through the observation of data, and then the power spectrum of fluctuating wind pressure can be estimated by the output power of parameter model method. This method is proposed for improving the bad resolution and variance performance in the classical spectral estimation. This paper adopts the minimizing prediction error autoregression (AR) spectral estimation in modern power spectral estimation, and an analysis of power spectrum is made in measuring non-Gaussian pulsating wind pressure for both the rigid and flexible structures with the fitted wind pressure autospectral formula in (2). The feature length L of flexible structure is selected as the height of the membrane, and the feature length L of rigid structure is chosen as the height of the rectangular masonry structure.

As shown in Figures 24 and 25, the power spectrum of the non-Gaussian fluctuating wind pressure measured on

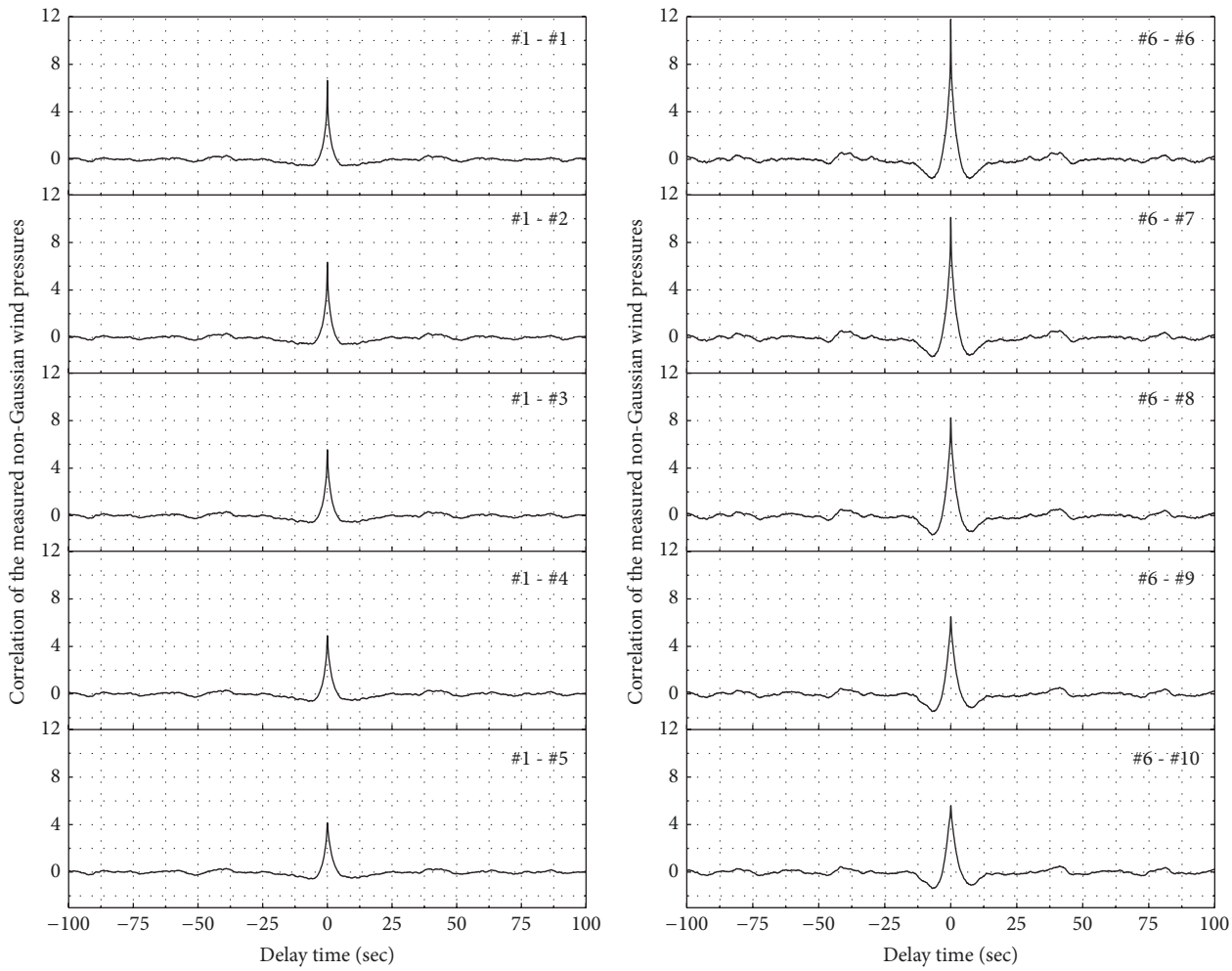

Figure 19: The correlation function of the measured non-Gaussian wind pressures (R1).

Table 3: The related parameters of measured fluctuating non-Gaussian wind pressures (R1).

Leeward side						Windward side					
Measuring points		X	A	B	β	Measuring points		X	A	B	β
Wall AB	#1	$X = L/U = 1.86/5.5 = 0.336$	12.39	254.3	1.022	Wall DA	#6	$X = L/U = 1.86/5.5 = 0.336$	31.02	414.6	1.044
	#2		16.65	304.9	1.033		#7		19.94	270.7	1.065
	#3		26.42	612.4	1.015		#8		84.26	1467	1.035
	#4		50.48	1469	1.002		#9		61.76	1356	1.024
	#5		17.59	528.7	1.028		#10		126.7	3672	1.007

the rigid structure fits nicely with (2); the parameters are shown in Tables 3 and 4. The parameter B has a large range from 10^2 to 10^5. Such phenomenon has been also found with other spectral models such as Kumar [23]. However, the parameter β has a stable range of values form 1.002 to 1.065, familiar with the identified parameter $\beta = 1$ in Pan [27]. As expected, the parameters of the wind pressure autospectral formula fitted with the flexible structure in Table 5 show different ranges and the power spectrum reveled in Figure 26 shows obvious error with (2). In order to find out a more appropriate empirical formula of the wind pressure autospectra for the flexible structure, Pan's autospectral formula [27] is utilized for fitting calculations as follows:

$$\frac{f \cdot S_P(f)}{\sigma_P^2} = \frac{A \cdot f \cdot X}{C + B(f \cdot X)^{10/3}}, \quad X = \frac{L}{U}. \tag{12}$$

However, the result of Pan's fitting autospectral formula for the flexible structure is even worse as shown in Figure 27.

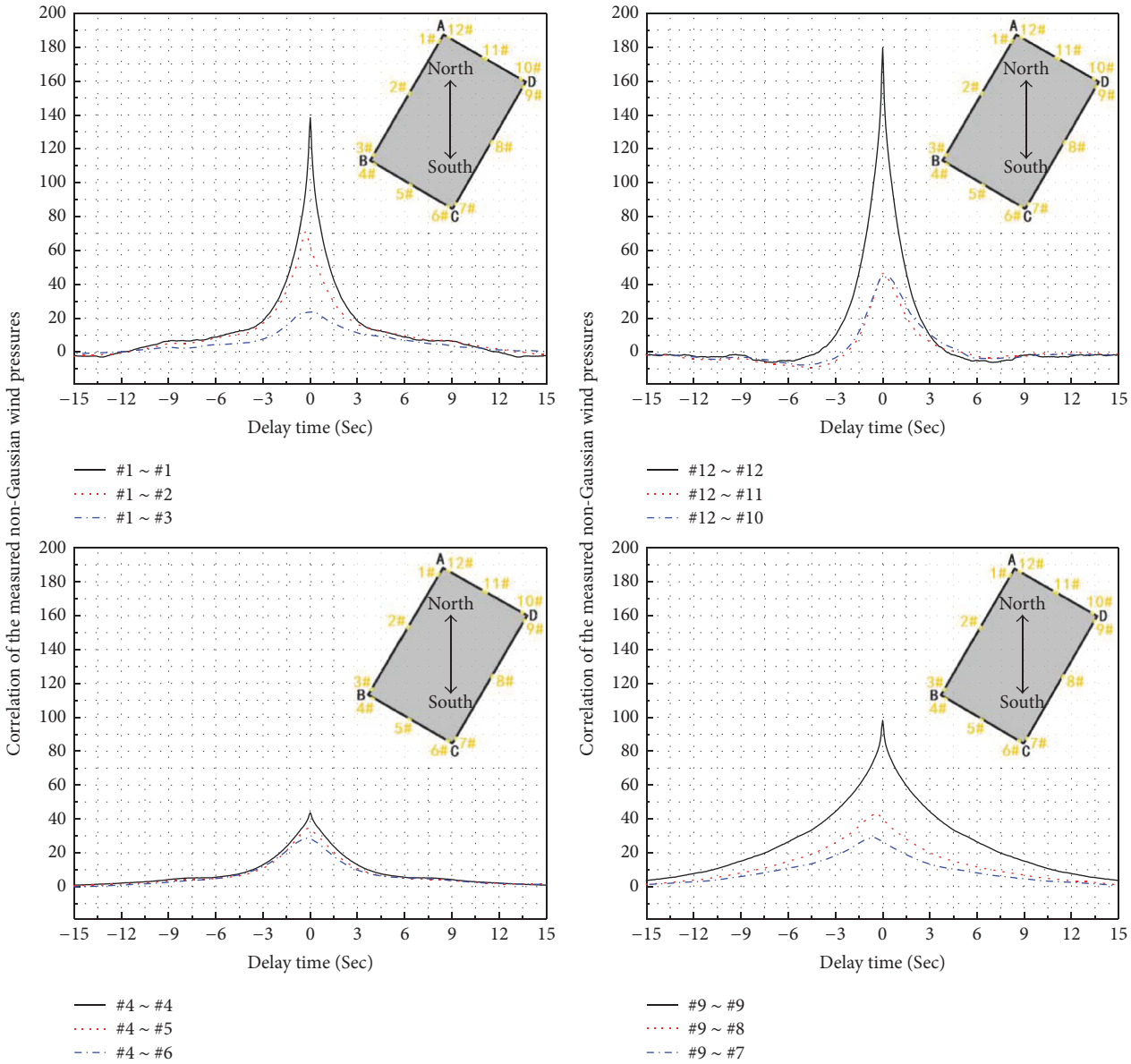

Figure 20: The correlation function of the measured non-Gaussian wind pressures (R2).

Table 4: The related parameters of measured fluctuating non-Gaussian wind pressures (R2).

Leeward side						Windward side					
Measuring points		X	A	B	β	Measuring points		X	A	B	β
Wall BC	#4	$X = L/U = 1.86/17.1 = 0.108$	845.8	99800	1.025	Wall AB	#1	$X = L/U = 1.86/17.1 = 0.108$	430.4	21790	1.019
	#5		1616	236300	1.031		#2		698	38390	1.034
	#6		1352	196000	1.038		#3		985	42850	1.014
Wall CD	#7		500.1	64950	1.034	Wall DA	#10		251.5	11630	1.03
	#8		389.4	46910	1.032		#11		280.4	13430	1.022
	#9		41.43	3292	1.044		#12		92.32	4021	1.016

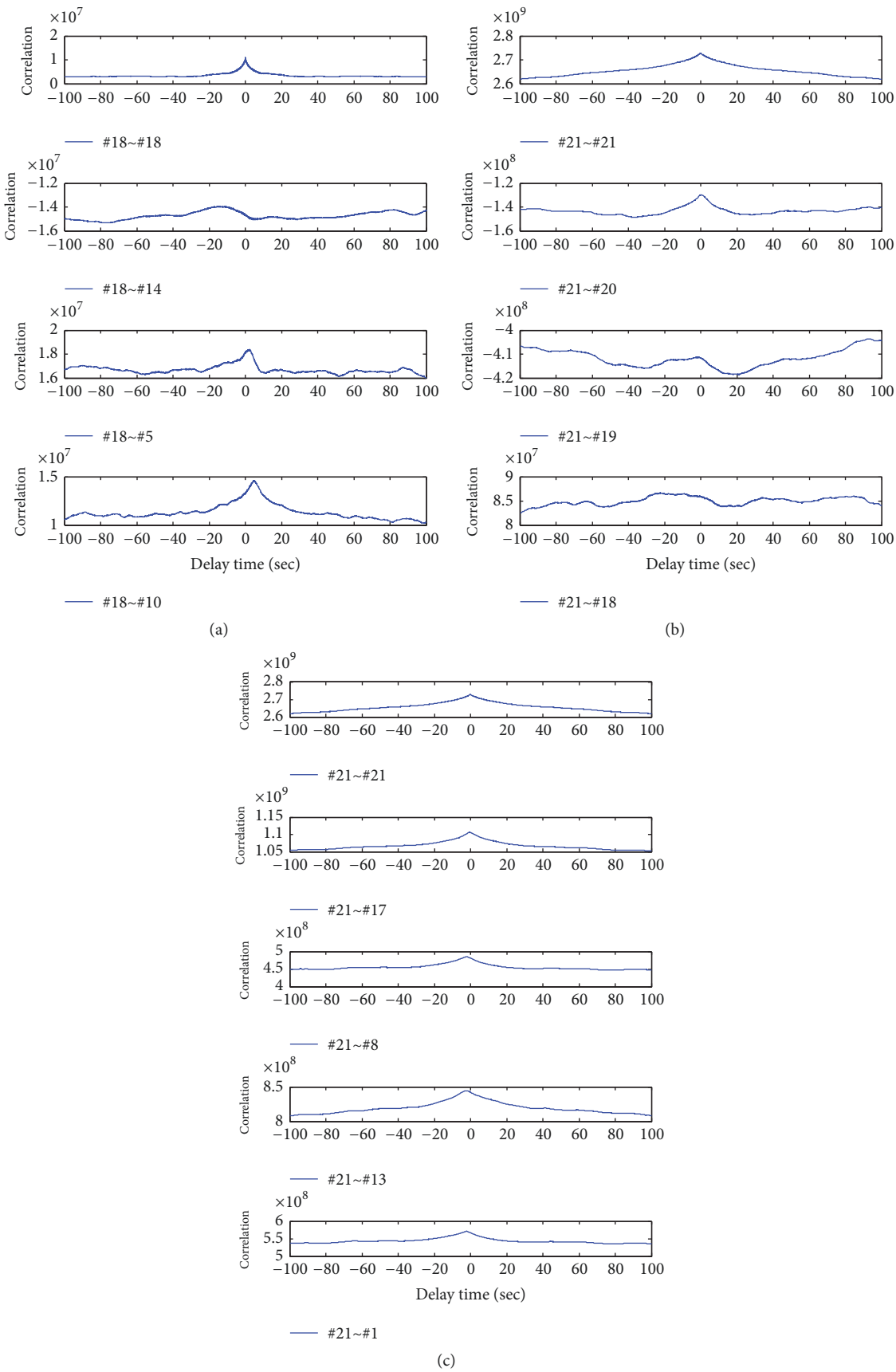

FIGURE 21: The correlation function of the measured non-Gaussian wind pressures (the flexible structure). (a) AD side (leeward side); (b) AB side; and (c) BC side (windward side).

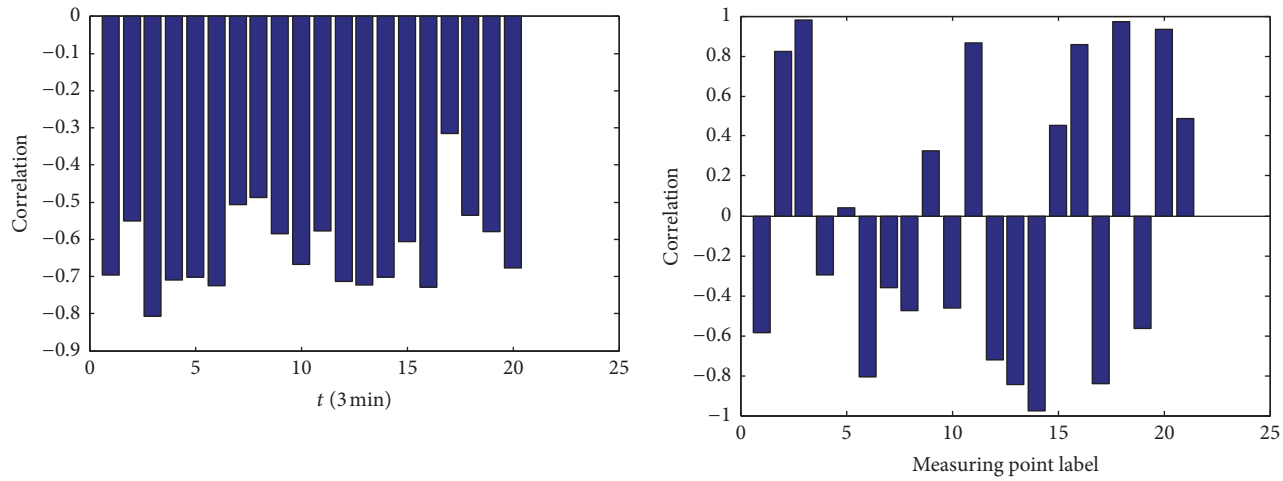

(a) (b)

Figure 22: The correlation of the wind pressures on upper and lower surface of the flexible structure. (a) The correlation coefficient of measurement point #1. (b) The correlation coefficient histogram of 21 measurement points.

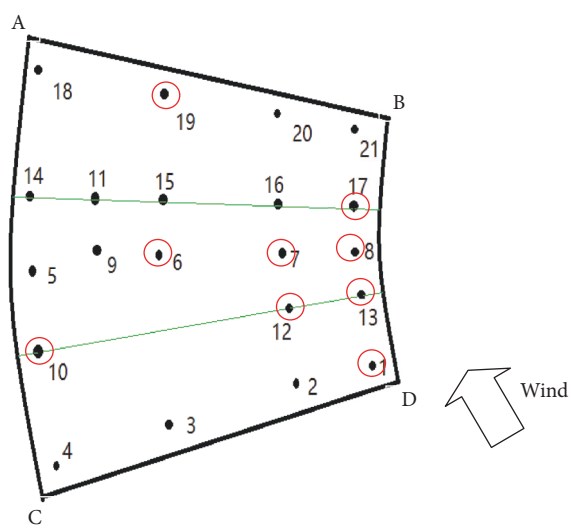

Figure 23: The measuring points with negative correlation coefficients.

Table 5: The related parameters of measured fluctuating non-Gaussian wind pressures (the flexible structure).

Windward side						Leeward side					
Measuring points		X	A	B	β	Measuring points		X	A	B	β
Wall AD	#1	9.23	1453	2634	0.932	Wall BC	#10	9.23	5087	4581	0.9096
	#13		7158	4117	0.9595		#5		15670	6670	0.9436
	#8		3636	3773	0.9264		#14		41670	9192	0.9458
	#17		1978	2698	0.956		#18		0.2976	0.2118	0.8034
	#21		1789	2615	0.9554						

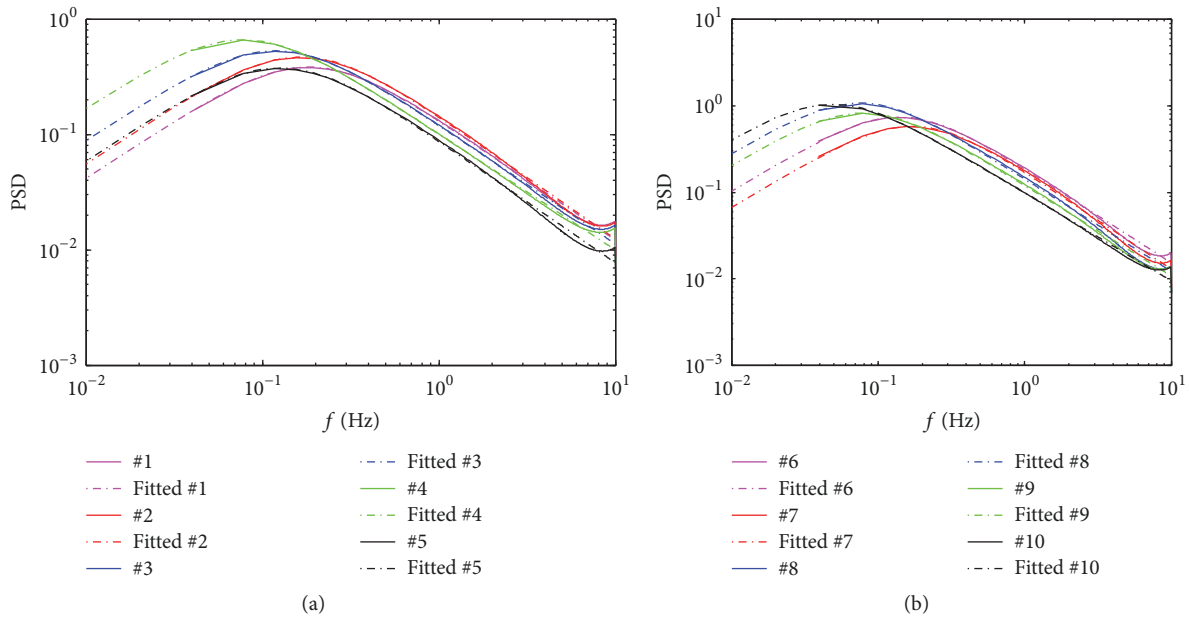

Figure 24: Power spectrum of measured fluctuating non-Gaussian wind pressures (R1).

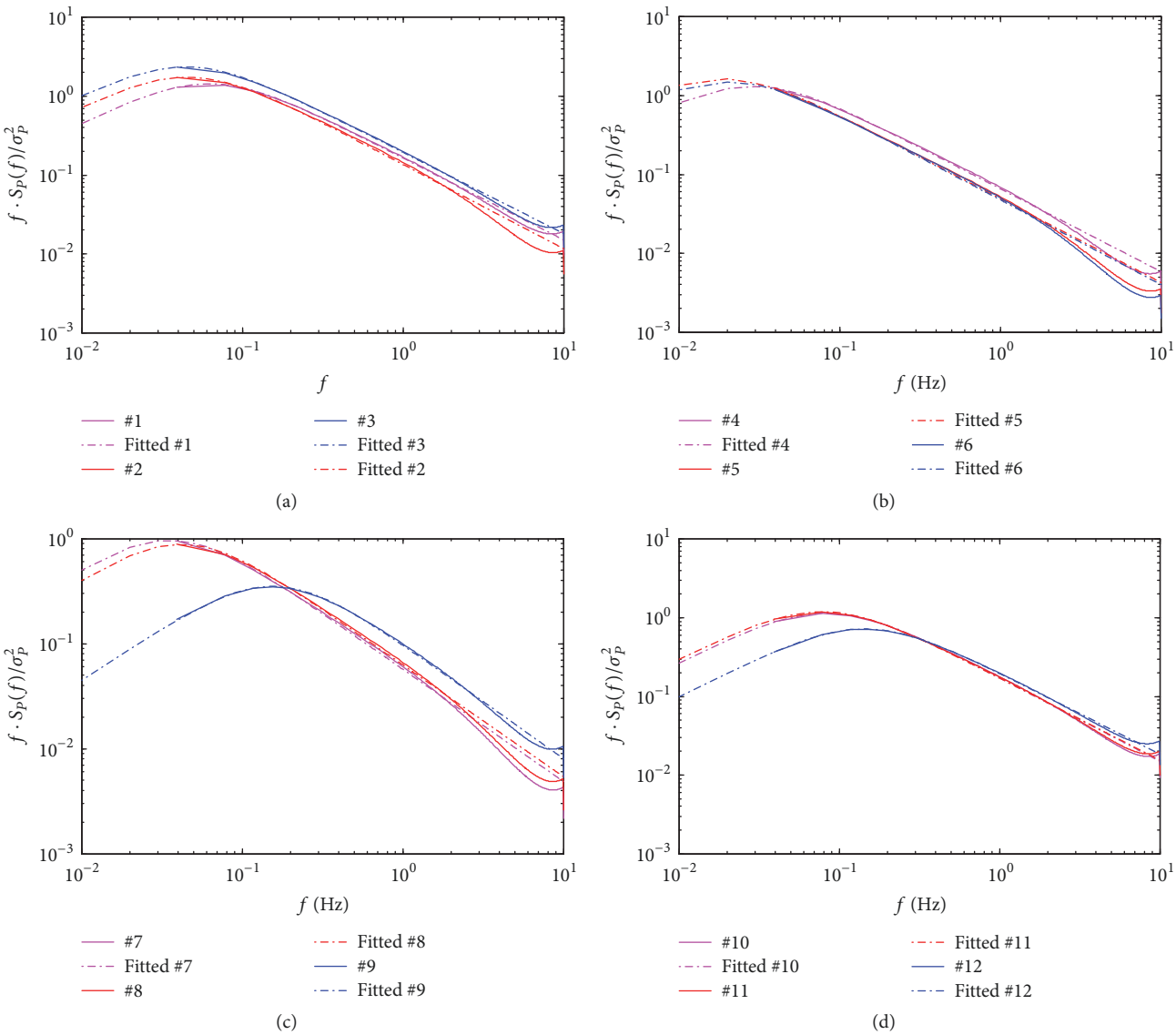

Figure 25: Power spectrum of measured fluctuating non-Gaussian wind pressures (R2).

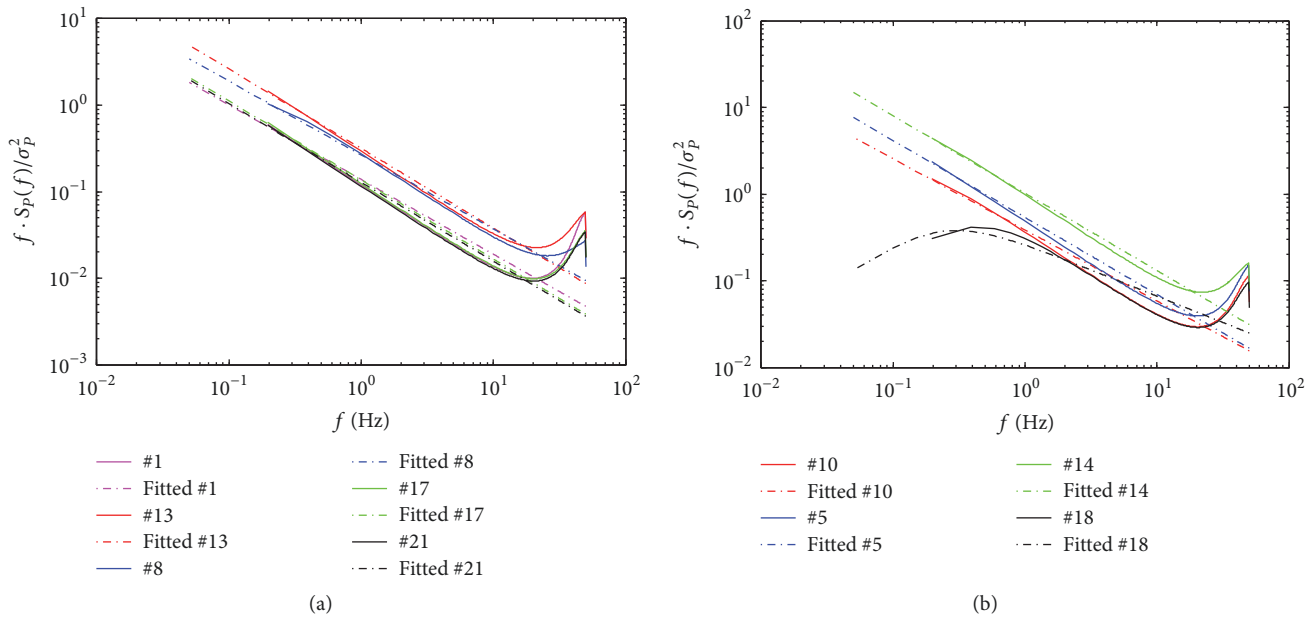

Figure 26: Power spectrum of measured fluctuating non-Gaussian wind pressures fitted with (11) (the flexible structure). (a) BC side and (b) AD side.

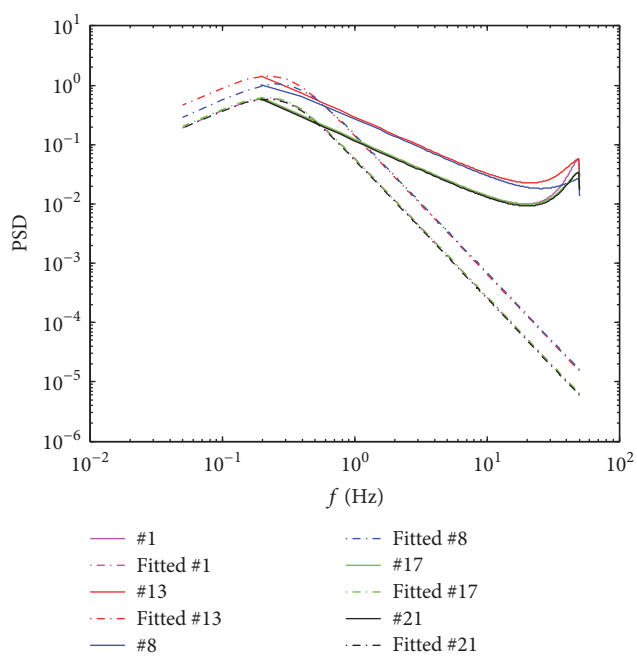

Figure 27: Power spectrum of measured fluctuating non-Gaussian wind pressures fitted with (12) (the flexible structure).

In summary, the present wind pressure autospectral formula cannot fit nicely with the PSD of the wind pressure for flexible structure, which will need further study.

5. Conclusion

In this paper, the non-Gaussian characteristics of measured pressure data were analyzed and discussed by comparing the measuring wind pressures on rigid structure and flexible structure, and the main conclusions are summarized as follows.

(1) From the analysis of PDF and high-order statistic characteristics of the wind pressure, the roof of flexible structure and the surface of rigid structure have some similarities that both of these two types of structure show softening non-Gaussian characteristics with kurtosis higher than 3, and the kurtosis always rapidly increases along with the increasing of the absolute value of the skewness. However, the difference between them is reflected as the roof of flexible structure shows strong non-Gaussian property in the windward side, while the surface of rigid structure shows non-Gaussian property mainly in the leeward.

(2) From the comparison of the wind pressure correlations between the rigid structure and flexible structure, some regularity results are found as follows: analysis of R1 and R2 tests shows that the correlation of wind pressures between measuring points on the windward side is stronger than that on the leeward side, which is also demonstrated in the flexible structure test. In addition, the wind pressures of the measuring points in parts of the flexible structure are negatively correlated and the time delay in the leeward side of the flexible structure is obvious.

(3) The correlation analysis of the measured wind pressure data of the upper and lower surface of the membrane structure is carried out. Most of the measuring points with negative correlation coefficients are close to the windward side; this type of negative correlation causes a bigger wind pressure root mean square coefficient Cp_{rms}. Therefore, when considering the structural wind load design value, the negative correlation area of wind pressure should be checked.

(4) This paper utilizes the present autospectrum empirical formula to fit the wind pressure power spectrum density of the measured data; the PSD of the rigid structure wind pressures can be fitted nicely; however, the existing empirical formula is not ideal for the fitting of the flexible structure, which needs further study.

Conflicts of Interest

The authors declare that they have no conflicts of interest.

Acknowledgments

The authors would like to acknowledge the financial contributions received from the National Natural Science Foundation of China (Grant no. 51378304) and the Science Foundation of Jiangxi Province (Grant no. 2017BAB206051). Also, the authors wish to thank Professor Zhi-hong Zhang for help in providing some figures presented in this paper and the precious wind pressure data for the flexible structure.

References

[1] W. A. Dalgliesh, "Comparison of model/full-scale wind pressures on a high-rise building," *Journal of Industrial Aerodynamics*, vol. 1, no. 3, pp. 55–66, 1975.

[2] J. D. Holmes, "Pressure fluctuations on a large building and along-wind structural loading," *Journal of Industrial Aerodynamics*, vol. 1, no. 3, pp. 249–278, 1975.

[3] T. Stathopoulos and D. Surry, "Scale effects in wind tunnel testing of low buildings," *Journal of Wind Engineering & Industrial Aerodynamics*, vol. 13, no. 1-3, pp. 313–326, 1983.

[4] K. S. Kumar and T. Stathopoulos, "Fatigue analysis of roof cladding under simulated wind loading," *Journal of Wind Engineering & Industrial Aerodynamics*, vol. 77-78, pp. 171–183, 1998.

[5] K. S. Kumar and T. Stathopoulos, "Synthesis of non-Gaussian wind pressure time series on low building roofs," *Engineering Structures*, vol. 21, no. 12, pp. 1086–1100, 1999.

[6] J.-H. Ye and X.-Z. Hou, "Non-Gaussian features of fluctuating wind pressures on long span roofs," *Journal of Vibration and Shock*, vol. 29, no. 7, pp. 9–15, 2010.

[7] K. S. Kumar and T. Stathopoulos, "Wind loads on low building roofs: a stochastic perspective," *Journal of Structural Engineering*, vol. 126, no. 8, pp. 944–956, 2000.

[8] X. L. Ma and F. Y. Xu, "Peak factor estimation of non-Gaussian wind pressure on high-rise buildings," in *Structural Design of Tall Special Buildings*, 2017.

[9] J. Li and C. Li, "Simulation of non-gaussian stochastic process with target power spectral density and lower-order moments," *Journal of Engineering Mechanics*, vol. 138, no. 5, pp. 391–404, 2012.

[10] M. D. Shields and G. Deodatis, "A simple and efficient methodology to approximate a general non-Gaussian stationary stochastic vector process by a translation process with applications in wind velocity simulation," *Probabilistic Engineering Mechanics*, vol. 31, pp. 19–29, 2013.

[11] L. Yang and K. R. Gurley, "Efficient stationary multivariate non-Gaussian simulation based on a Hermite PDF model," *Probabilistic Engineering Mechanics*, vol. 42, pp. 31–41, 2015.

[12] S. Ke and Y. Ge, "Extreme wind pressures and non-gaussian characteristics for super-large hyperbolic cooling towers considering aeroelastic effect," *Journal of Engineering Mechanics*, vol. 141, no. 7, pp. 1–12, 2015.

[13] Q. Yang and Y. Tian, "A model of probability density function of non-Gaussian wind pressure with multiple samples," *Journal of Wind Engineering & Industrial Aerodynamics*, vol. 140, pp. 67–78, 2015.

[14] W.-J. Lou, J.-X. Li, G.-H. Shen, and M.-F. Huang, "Non-Gaussian feature of wind-induced pressure on super-tall building," *Journal of Zhejiang University (Engineering Science)*, vol. 45, no. 4, pp. 671–677, 2011.

[15] N. Han and M. Gu, "Analysis on non-Gaussian features of fluctuating wind pressure on square tall buildings," *Journal of Tongji University*, vol. 40, no. 7, pp. 971–976, 2012.

[16] J. Ding and X. Z. Chen, "Moment-based translation model for hardening non-Gaussian response processes," *Journal of Engineering Mechanics*, vol. 142, no. 2, pp. 1–7, 2016.

[17] X. Ma, F. Xu, A. Kareem, and T. Chen, "Estimation of surface pressure extremes: Hybrid data and simulation-based approach," *Journal of Engineering Mechanics*, vol. 142, no. 10, Article ID 04016068, 2016.

[18] Q. S. Li, Y. J. Wang, and J. C. Li, "Monitoring of wind effects on an instrumented low-rise building during the landfall of a severe tropical storm," *Structural Control and Health Monitoring*, 2016.

[19] M. Bartko, S. Molleti, and A. Baskaran, "In situ measurements of wind pressures on low slope membrane roofs," *Journal of Wind Engineering & Industrial Aerodynamics*, vol. 153, pp. 78–91, 2016.

[20] F. Liang, J. Xian, and J. Wang, "Wind-induced dynamic analysis of rung-shape long-span tensile cable membrane structure," *Applied Mechanics and Materials*, vol. 578-579, pp. 432–440, 2014.

[21] D. Zheng, M. Gu, X. Zhou, W. Zhang, W. Fang, and A. Zhang, "Numerical simulation of mean wind pressure on membrane roof of EXPO-axis," *Journal of Building Structures*, vol. 30, no. 5, pp. 212–219, 2009.

[22] J. Luo, X. Song, and J. Li, "Wind-induced response analysis on a large-span membrane roof by considering non-Gaussian stochastic wind pressure field," *Journal of Civil Architectural and Environmental Engineering*, vol. 35, no. 6, pp. 118–123, 2013.

[23] K. S. Kumar, *Simulation of Fluctuating Wind Pressures on Low Building Roofs (PhD thesis)*, Concordia University, Montreal, Canada, 1997.

[24] Y. Tamura, H. Kawai, Y. Uematsu, H. Marukawa, K. Fujii, and Y. Taniike, "Wind load and wind-induced response estimations in the Recommendations for loads on buildings," *Engineering Structures*, vol. 18, no. 6, pp. 399–411, 1996.

[25] Y. Uematsu, M. Yamada, and A. Karasu, "Design wind loads for structural frames of flat long-span roofs: Gust loading factor for the beams supporting roofs," *Journal of Wind Engineering & Industrial Aerodynamics*, vol. 66, no. 1, pp. 35–50, 1997.

[26] Y. Sun, *Characteristics of Wind Loading on Long-span Roofs (PhD thesis)*, Harbin Institute of Technology, 2007 (Chinese).

[27] F. Pan, *Refinement Theory of Random Wind-Induced Dynamic Response for Long-Span Roof Structures (PhD thesis)*, Zhejiang University, Hangzhou, China, 2008 (Chinese).

[28] Y. Uematsu and R. Tsuruishi, "Wind load evaluation system for the design of roof cladding of spherical domes," *Journal of Wind Engineering & Industrial Aerodynamics*, vol. 96, no. 10-11, pp. 2054–2066, 2008.

[29] L. Li, Y. Xiao, A. Kareem, L. Song, and P. Qin, "Modeling typhoon wind power spectra near sea surface based on measurements in the South China sea," *Journal of Wind Engineering & Industrial Aerodynamics*, vol. 104-106, pp. 565–576, 2012.

[30] N. Su, Y. Sun, Y. Wu, and S. Shen, "Three-parameter auto-spectral model of wind pressure for wind-induced response analysis on large-span roofs," *Journal of Wind Engineering and Industrial Aerodynamics*, vol. 158, pp. 139–153, 2016.

[31] H. R. Olesen, S. E. Larsen, and J. Højstrup, "Modelling velocity spectra in the lower part of the planetary boundary layer," *Boundary Layer Meteorology*, vol. 29, no. 3, pp. 285–312, 1984.

[32] H. W. Tieleman, "Universality of velocity spectra," *Journal of Wind Engineering & Industrial Aerodynamics*, vol. 56, no. 1, pp. 55–69, 1995.

[33] Y. Sun, Y. Qiu, and Y. Wu, "Modeling of wind pressure spectra on spherical domes," *International Journal of Space Structures*, vol. 28, no. 2, pp. 87–100, 2013.

[34] Y. Sun, N. Su, and Y. Wu, "Modeling of conical vortex induced fluctuating wind pressure spectra on large-span flat roofs," *China Civ. Eng. J*, vol. 47, no. 1, pp. 87–98, 2014 (Chinese).

[35] S. Shao, *Research on Wind Load Characteristics and Interference Effects of Arc Cantilevered Stadium Roofs (M. S. thesis)*, Harbin Institute of Technology, Harbin, China, 2013 (Chinese).

[36] M. Gioffrè, V. Gusella, and M. Grigoriu, "Non-Gaussian wind pressure on prismatic buildings. I: Stochastic field," *Journal of Structural Engineering*, vol. 127, no. 9, pp. 981–989, 2001.

[37] Z. Zhi-hong, L. Zhong-hua, and D. Shi-lin, "Field measurement of wind pressure and wind-induced vibration of large-span spatial cable-truss system under strong wind or typhoon," *Journal of Shanghai Normal University (Natural Sciences)*, vol. 42, no. 5, pp. 546–550, 2013 (Chinese).

[38] M. Rhudy, B. Bucci, J. Vipperman, J. Allanach, and B. Abraham, "Microphone array analysis methods using cross-correlations," in *Proceedings of the 2009 ASME International Mechanical Engineering Congress and Exposition, (IMECE '09)*, pp. 281–288, USA, November 2009.

[39] Z. Liang and et al., *Probability Theory and Mathematical Statistics*, Higher Education Press, Beijing, China, 1988.